Query Details

Back to Main Page

1. A proof will be produced on the basis of your corrections to this preproof. For this later stage of production we use an online 'eproof' tool, where you can make corrections directly to the text within the tool and also mark up corrections to the copyedited figures. You will receive a link to the eproof tool via email later in the production process. When you receive the eproof link, please check that the display items are as follows (ms no: 2019-02-03175D): Figs none (black & white); 6 (colour); Tables: None; Boxes: None; Extended Data display items: 10; SI: yes. The eproof contains the main-text figures edited by us and (if present) the Extended Data items (unedited except for the legends) and the Supplementary Information (unedited). Please note that the eproof should be amended in only one browser window at any one time, otherwise changes will be overwritten. Please check the edits to all main-text figures (and tables, if any) very carefully, and ensure that any error bars in the figures are defined in the figure legends. Extended Data items may be revised only if there are errors in the original submissions. If you need to revise any Extended Data items please upload these files when you submit your corrections to this preproof . • A single sentence summarizing your paper (websum), which will appear online on the table of contents and in e-alerts, has been provided below. Please check this sentence for accuracy and appropriate emphasis.

We preffered the new title: "Patch repair of deep wounds by mobilized fascia"

We suggest the following sentence for the editor's summary:
"Skin scars originate from cells and prefabricated matrix in the subcutaneous fascia that home into wounds."

2. There must be a city for each affiliation, so we have added Munich for German Centre for Lung Research. OK?

That's OK

3. Please check your article carefully, coordinate with any co-authors and enter all final edits clearly in the eproof, remembering to save frequently. Once corrections are submitted, we cannot routinely make further changes to the article.

OK

4. Note that the eproof should be amended in only one browser window at any one time; otherwise changes will be overwritten.

OK

5. Author surnames have been highlighted. Please check these carefully and adjust if the first name or surname is marked up incorrectly. Note that changes here will affect indexing of your article in public repositories such as PubMed. Also, carefully check the spelling and numbering of all author names and affiliations, and the corresponding email address(es).

Done

6. You cannot alter accepted Supplementary Information files except for critical changes to scientific content. If you do resupply any files, please also provide a brief (but complete) list of changes.

No additional or resupplied files are included

7. **Please define ep as used in Fig. 4c.**

ep, epidermis

Patch repair of deep wounds by mobilized fascia Fascia is a repository of mobile scar tissue

Donovan Correa-Gallegos, [1]

Dongsheng Jiang, [1]

Simon Christ, [1]

Pushkar Ramesh, [1]

Haifeng Ye, [1]

Juliane Wannemacher, [1]

Shruthi Kalgudde Gopal, [1]

Qing Yu, [1]

Michaela Aichler, [2]

Axel Walch, [2]

Ursula Mirastschijski, [3,4]

Thomas Volz, [5]

Yuval Rinkevich, [1]✉,[6]

Email yuval.rinkevich@helmholtz-muenchen.de

[1] Group Regenerative Biology and Medicine, Institute of Lung Biology and Disease, Helmholtz Zentrum München, Munich, Germany

[2] Research Unit Analytical Pathology, Helmholtz Zentrum München, Munich, Germany

[3] Mira-Beau Gender Esthetics, Berlin, Germany

[4] Wound Repair Unit, CBIB, Department of Biology and Biochemistry, University of Bremen, Bremen, Germany

[5] Department of Dermatology and Allergology, School of Medicine, Klinikum rechts der Isar, Technical University of Munich, Munich, Germany

[6] German Centre for Lung Research (DZL), Munich, Germany

Received: 28 February 2019 / Accepted: 30 October 2019

Abstract

Mammals form scars to quickly seal wounds and ensure survival by an incompletely understood mechanism[1, 2, 3, 4, 5]. Here we show that skin scars originate from prefabricated matrix in the subcutaneous fascia. Fate mapping and live imaging revealed that fascia fibroblasts rise to the skin surface after wounding, dragging their surrounding extracellular jelly-like matrix, including embedded blood vessels, macrophages and peripheral nerves, to form the provisional matrix. Genetic ablation of fascia fibroblasts prevented matrix from homing into wounds and resulted in defective scars, whereas placing an impermeable film beneath the skin—preventing fascia fibroblasts from migrating upwards—led to chronic open wounds. Thus, fascia contains a specialized prefabricated kit of sentry fibroblasts, embedded within a movable sealant, that preassemble together diverse cell types and matrix components needed to heal wounds. Our findings suggest that chronic and excessive skin wounds may be attributed to the mobility of the fascia matrix.

AQ1

AQ2

Editor's Summary

Cells that populate scar tissue in mammalian skin migrate as prefabricated matrix from the subcutaneous fascia, including embedded blood vessels, macrophages and peripheral nerves.Skin scars originate from cells and prefabricated matrix in the subcutaneous fascia that home into wounds.

These authors contributed equally: Donovan Correa-Gallegos, Dongsheng Jiang

Main

Mammalian scarring occurs when specialized fibroblasts migrate into wounds to deposit plugs of extracellular matrix[1]. Abnormal scarring results in either non-healing chronic wounds or aggravating fibrosis[2, 3, 4], which represent a high burden for patients and to the global healthcare system. In the US alone, costs related to impaired scarring amount to tens of billions of dollars per year[5].

AQ3

AQ4

AQ5

AQ6

The origin of fibroblasts in wounds and the mechanism by which they act remain unclear[6]. Possible sources, such as papillary (upper) and reticular (lower) dermal layers[7], pericytes[8], adipocytes[9, 10] and bone-marrow derived monocytes[11] have been suggested. We previously demonstrated that all scars in the back skin derive from a distinct fibroblast lineage expressing the engrailed 1 gene (*En1*) during embryogenesis and we refer to these cells as En1-lineage positive fibroblasts (EPFs)[12, 13]. This lineage is present not only in the skin but also in the strata underneath, called fascia.

The fascia is a gelatinous viscoelastic membranous sheet that creates a frictionless gliding interface between the skin and the body's rigid structure below. Mouse back-skin fascia extends as a single sheet separated from the skin by the Panniculus carnosus (PC) muscle, whereas in humans back-skin there is no intervening muscle and the fascia consists of several thicker sheets that are continuous with the skin. In humans the facia layers incorporate fibroblasts, lymphatics, adipose tissue, neurovascular sheets and sensory neurons[14, 15].

Here we explored the fundamental mechanisms of scar formation by using matrix-tracing techniques, live imaging, genetic-lineage tracing and anatomic fate-mapping models. We identified the fascia as a major source of wound-native cells, including fibroblasts. Notably, we found that wound provisional matrix originates from prefabricated matrix in the fascia that homes in to open wounds as a movable sealant dragging along vasculature, immune cells and nerves, upwards into the skin.

Wound cells rise from fascia

To trace the origins of cells in wounds, we developed a fate-mapping technique by transplanting chimeric skin and fascia grafts into living animals (Fig. 1a and Methods).

Fig. 1

Fascia is a major cellular source for wounds.

a, Generation of 6-mm diameter chimeric grafts with an inner 2-mm wound to determine contributions of dermis and fascia. **b**, Percentages of TdTomato^{+} or GFP^{+} cells from total labelled cells in the wound and wound margin. Data are mean ± s.e.m., n = 26 images from 4 biological replicates. One-way ANOVA, multiple comparison Tukey's test, 95% confidence interval (CI). **c**, Wound showing skin- and fascia-derived cells at 14 dpw. **d**, **e**, Immunolabelling and contributions of myofibroblasts (ACTA2), nerves (TUBB3), blood vessels (PECAM1), monocytes or macrophages (MOMA-2) and lymphatic cells (LYVE1). Data are mean ± s.e.m.; n = 4 (LYVE1), 5 (ACTA2, TUBB3 and MOMA-2) or 8 (PECAM1) images from 4 biological replicates. Unpaired two-tailed t-test, 95% CI. Dotted lines delimit the wound. Arrowheads indicate injury site. Scale bars, 200 μm. TdTom, TdTomato.

Source data

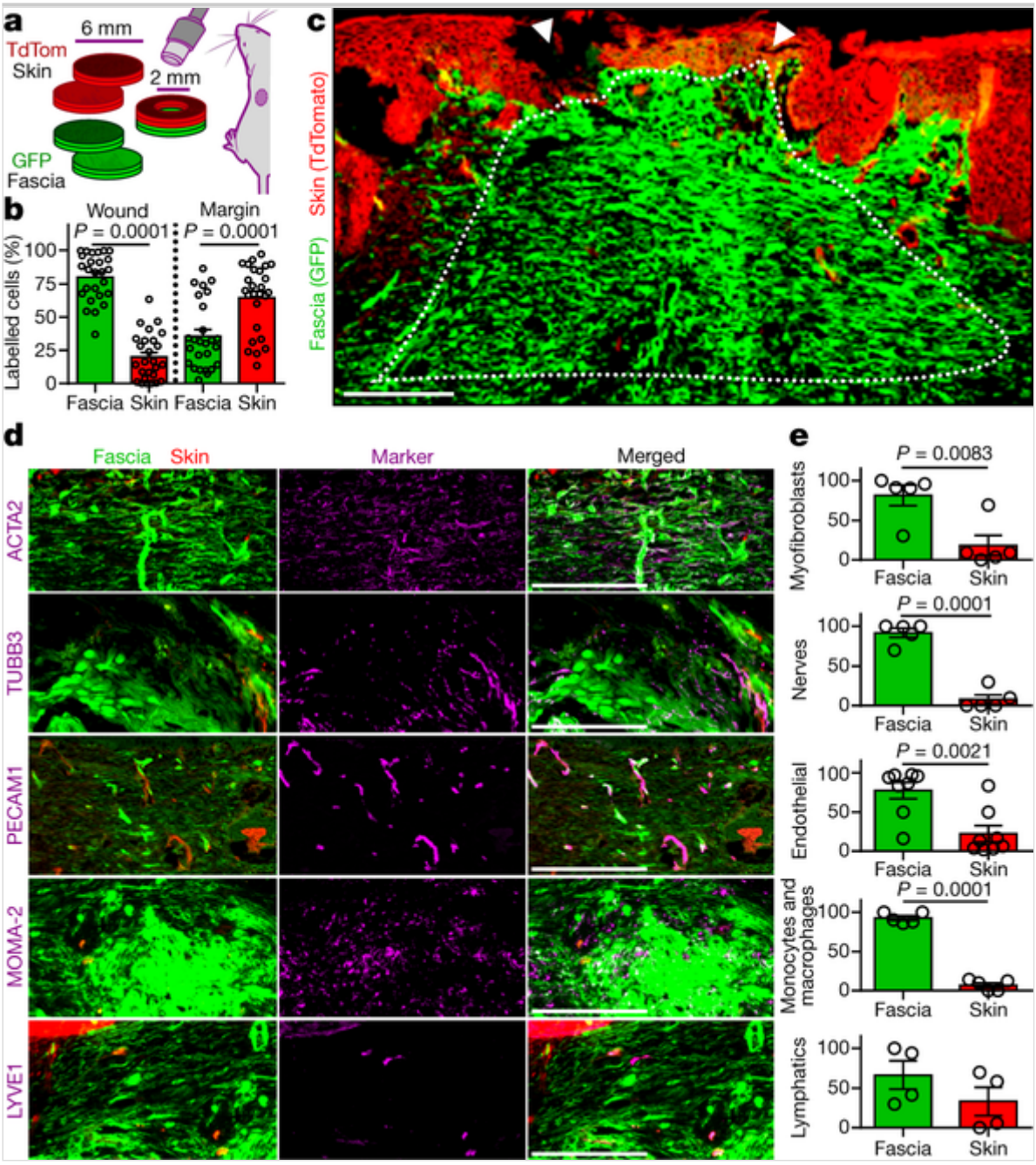

At 14 days post-wounding (dpw), 80.04 ± 3.443% (mean ± s.e.m.) of the labelled cells in the wound originated from fascia (Fig. 1b). Fascia-derived cells filled the entire wound bordering the regenerated epidermis and even the surrounding dermis, making up 35.46 ± 4.938% of the total labelled cells within a 0.2 mm radius (Fig. 1b, c). $ACTA2^{+}$ myofibroblasts (81.63 ± 12.84%), nerve cells, endothelial cells and macrophages within wounds were predominantly of fascia origin (Fig. 1d, e). Independently, in vivo labelling of the fascia showed same results (Extended Data Fig. 1a, Methods). Labelled cells populated the wounds and surrounding dermis at 14 dpw, whereas in uninjured controls, labelled cells remained in the fascia (Extended Data Fig. 1b). Up to 56.71 ± 9.319% of fascia-derived cells in wounds expressed classical fibroblast markers (Extended Data Fig. 1c). Labelled monocytes (macrophages), lymphatics, endothelium and nerves also derived from fascia (Extended Data

Fig. 1d). Collectively, our two independent fate-mapping approaches demonstrate that fascia is a major reservoir of fibroblasts, endothelial cells macrophages and peripheral nerves that populate wounds following injury.

Fascia fibroblasts dictate scar severity

We then analysed the scar-forming EPFs across dermal and fascia compartments by using a TdTomato-to-GFP replacement reporter[12, 13] ($En1^{Cre}$;$R26^{mTmG}$; see Methods). Fibroblasts were the predominant fascia cell type (71.1%), whereas dermis had a significantly lower fraction of fibroblasts (56.4%, Extended Data Fig. 2a, b). Within this population, there were twice as many EPFs as En1-naive fibroblasts (ENFs) in the fascia (61.2% and 31.8%, respectively). In dermis, there was a sixfold excess of EPFs (83.13% EPFs versus 12.78% ENFs; Extended Data Fig. 2c, d). Fascia was also enriched in regenerative cell types such as endothelial cells and lymphatics, whereas populations of macrophages and nerve cells were similar in both compartments (Extended Data Fig. 2e). Thus, a higher proportion of fibroblasts, endothelial cells and lymphatic cells and a lower EPF to ENF ratio distinguishes the fascia from dermis.

Two-photon microscopy revealed that fascia EPFs assemble in monolayers of consecutive perpendicular sheets across the dorsal–ventral axis (Extended Data Fig. 2f, Supplementary Video 1). EPFs populate the entire back in topographic continua extending from the fascia and traversing the PC (Extended Data Fig. 2g, h Supplementary Video 2). Regions where PC ended or where nerve bundles and blood vessels traversed the PC also showed continuums of EPFs without clear boundaries (Extended Data Fig. 2i, j). To test whether fascia EPFs could access dermal layers upon injury, we generated superficial excisional wounds. Aggregates of EPFs rising into open wounds from fissures in the PC were observed after only 3 dpw (Extended Data Fig. 2k, Supplementary Video 3). Collectively, our observations suggest that fascia EPFs easily traverse upwards into dermal layers during wounding and are unobstructed by the PC muscle.

The size of a scar increases with the depth of the injury[16]. We therefore investigated whether this correlation can be attributed to fascia by analysing the extent of fibroblast contributions from the fascia and dermis in deep versus superficial wounds. For this, we combined genetic lineage-tracing ($En1^{Cre}$;$R26^{mTmG}$) with our anatomic fate-mapping chimeric grafts and inflicted superficial or deep injuries (Fig. 2a, Methods). Fourteen days post-wounding, mean wound size of deep injuries was 1.7 times that of superficial injuries (Fig. 2b, c). There were twice as many fascia EPFs in deep wounds, whereas the number of dermal EPFs remained constant in both conditions (Fig. 2d). The

abundance of fascia EPFs in the wound directly correlated with wound size and thus scar severity, whereas dermal EPFs showed no such correlation (Fig. 2e, f). No crossing of EPFs between these compartments was observed in uninjured controls, indicating that the influx of fascia EPFs was triggered by injury (Extended Data Fig. 3a, b).

Fig. 2

Fascia EPFs dictate scar severity.

a, Dermal versus fascia EPFs chimeric grafts. Chimeric grafts were prepared as in Fig. 1a, using the EPF reporter line $En1^{cre};R26^{mTmG}$ combined with cre-negative littermate samples to trace EPFs in each compartment. **b**, Images showing fascia EPFs (left) or dermal EPFs (right) in wounds after a deep (top) or superficial injury (bottom). **c**, Wound size. Data are mean ± s.e.m.; n = 70 (deep) and 53 (superficial) images analysed from 5 biological replicates. Unpaired, two-tailed t-test, 95% CI. **d**, Numbers of fascia and dermal EPFs. Data are mean ± s.e.m.; n = 27, 32, 27 and 22 images analysed from 5 biological replicates. Unpaired, two-tailed t-test, 95% CI. **e**, **f**, Plots of EPF fractions and wound size from fascia (**e**) and dermal EPFs (**f**). n = 57 (**e**) and 48 (**f**) images analysed from 5 biological replicates. Two-tailed Pearson's R^2 correlation, 95% CI. Dotted lines delimit wounds. Scale bars, 200 μm.
Source data

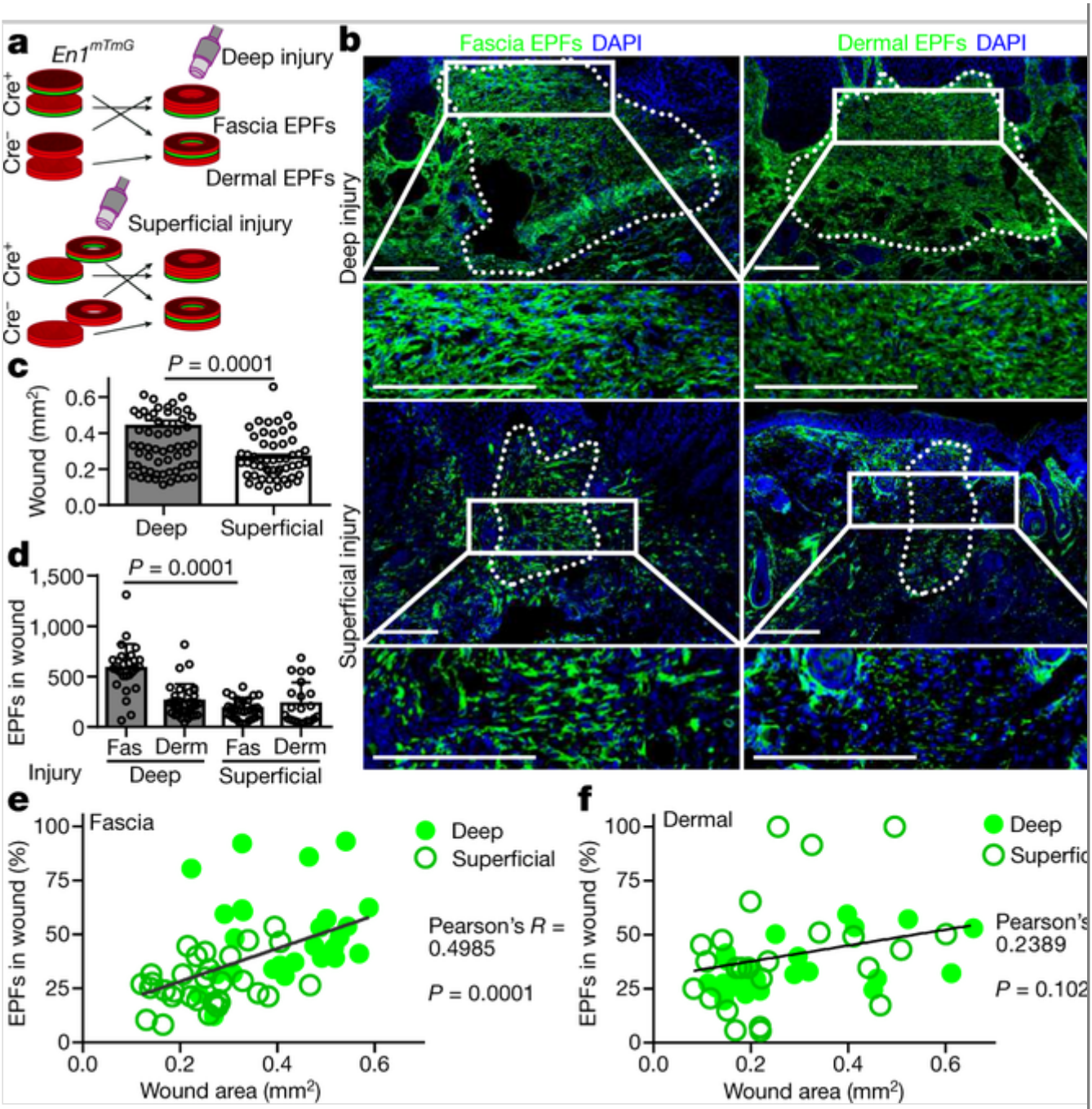

Long-term tracing of fascia EPFs in wounds showed that they recede ten weeks after injury (Extended Data Fig. 3c). This desertion from mature scars occurred through an apoptosis-independent mechanism, indicated by a low rate of cell death (<5%) across earlier time points (Extended Data Fig. 3d, e).

We next sought to place fascia EPFs in the framework of known lineage markers used to define different populations of wound fibroblasts such as CD24, CD34, DPP4, DLK1 and LY6A[7, 10, 12]. All markers were prominent in fascia EPFs and were surprisingly downregulated upon entering the wound in our graft experiments (Extended Data Fig. 4). Flow cytometry confirmed the higher expression of DPP4, ITGB1, LY6A and PDGFRα in fascia than in dermal fibroblasts (Extended Data Fig. 5a–c). Sorted fascia EPFs also revealed low cellular heterogeneity, with the population predominantly comprising

LY6G$^+$PDGFRα$^+$ (87.0%) and DPP4$^+$ITGB1$^+$ (72.8%) cells (Extended Data Fig. 5d). This broad marker convergence identifies fascia EPFs as the major source of wound fibroblasts.

Provisional matrix emerges from fascia matrix

We then looked at the fascia matrix itself. Second harmonic generation (SHG) signal and scanning electron micrographs (SEM) revealed profuse coiled collagen fibrils in the fascia, indicative of a relaxed and immature matrix (Fig. 3a, b). Fractal measurements[13] of the fibre alignments showed a more condensed matrix configuration in fascia than the stretched and woven dermal matrix (Fig. 3c).

Fig. 3

Fascia matrix steers into wounds.

a, SHG (**a**) and SEM images (**b**) of fascia (left) and dermis (right) showing matrix arrangements, representative images of 3 biological replicates. **c**, Fractal dimension and lacunarity values from SHG images. $n = 6$ (dermis) and 3 (fascia) images analysed from 3 biological replicates. Unpaired two-tailed *t*-test, 95% CI. **d**, Time-lapse images of fascia in culture at time 0 (left) and 30 h (right). Representative video from at least three independent experiments. Autof., autofluorescence. **e**, Contraction rate from the SHG and autofluorescence. Data derived from Supplementary Video 4. **f**, Fascia matrix labelling with AF647 NHS ester in chimeric grafts. TdTomato and GFP reporter lines biopsies were used for the chimeric grafts as before. Only the matrix of the GFP-positive fascia compartment was labelled prior transplantation. **g**, Images at 7 dpw showing fascia matrix covering the wound. Representative image of at least three biological replicates. **h**, In situ fascia matrix-tracing experiment using FITC NHS ester. Subcutaneous injections of FITC NHS ester were performed 4 and 2 days before wounding in the back-skin of wild-type mice to label the fascia matrix. **i**, Uninjured controls showing specificity of the labelling in fascia. Representative sample of at least three biological replicates. **j**, Images from 7 dpw showing fascia matrix covering the wound area. Representative samples of at least three biological replicates. Arrowheads indicate the original injury. Broken lines delimit dermis (**g** and **j**) or PC (**i**). Scale bars: 30 μm (**a**, **b**), 500 μm (**d**, **g**, **i**, **j**), and 100 μm (**g**, **j** magnified insets).

Source data

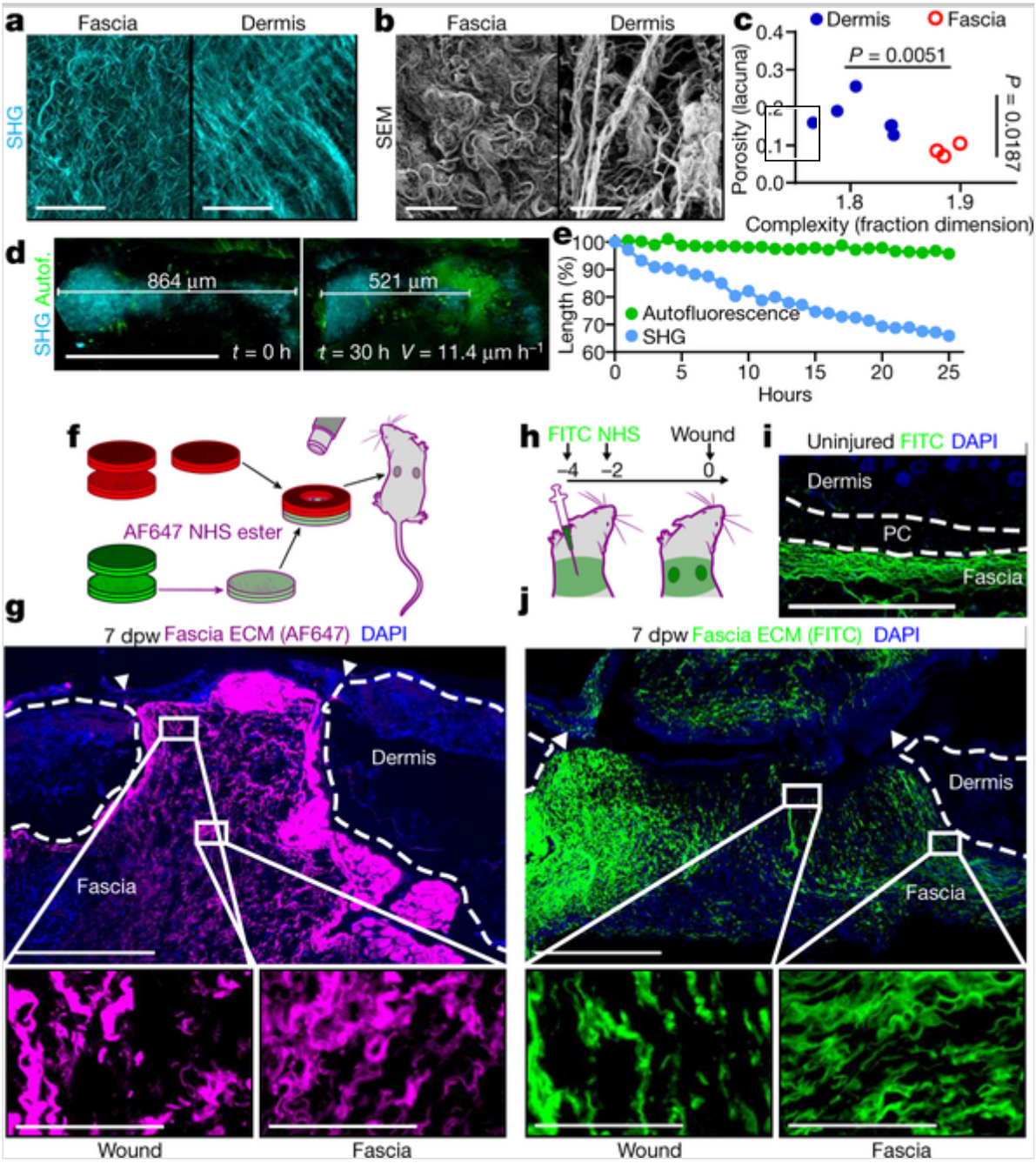

Given the immaturity of the fascia matrix, we checked whether it could work as a repository for scar tissue. We developed an incubation chamber that enabled live imaging of fascia biopsies over several days (Methods). Recording of SHG signals showed steering of the matrix at a rate of 11.4 µm h^{-1} (Fig. 3d, e, Supplementary Video 4). Assuming a similar rate in vivo, the fascia matrix could move about 2 mm in 7 days, accounting for the dynamics of provisional matrix deposition in mammals.

To test whether fascia matrix steers into wounds in vivo, we developed a method to trace the fascia matrix in our chimeric grafts using NHS esters. (Fig. 3f, Methods). Streams of traced matrix from the fascia extended upwards and plugged the open wounds from 7 dpw (Fig. 3g, Extended Data Fig. 6a, b). Fascia-derived matrix covered 74.78 ± 12.94% of total collagen content in the

wound (Extended Data Fig. 6c). Our data indicated that individual fascia matrix fibres were not being pulled; instead, pliable matrix was extended upwards to mould the wound. Advanced wound stages showed a decline in label in specific regions of the wound, suggesting an active remodelling process of the fascia-derived matrix (Extended Data Fig. 6d–f, Supplementary Video 5).

We then tested whether dermal matrix could be steered by double labelling our chimeric grafts. Only the fascia matrix plugged deep injury wounds (Extended Data Fig. 6g–j), whereas dermal matrix remained immobile in deep and superficial injuries; the superficial injuries healed via de novo matrix deposition (Extended Data Fig. 6k, l).

To provide further evidence showing that fascia matrix migrates to open wounds, we labelled the fascia matrix in situ before injury (Fig. 3h, i, Methods). Labelled matrix made up most of the wound provisional matrix (Fig. 3j), which underwent remodelling during the first two weeks following injury (Extended Data Fig. 7a, b). Fractal measurements showed that fascia fibre interfaces expanded by 3 dpw, changing from a parallel sheet arrangement to a highly porous plug. This expansion was followed by contraction into thicker and more complex mature scar matrix architecture (Extended Data Fig. 7c–e). Surprisingly, traced matrix was also present in the eschar. Activated platelets infiltrated and clustered within fascia fibres before eschar formation (Extended Data Fig. 7f), indicating that the coagulation cascade occurs in parallel with fascia matrix steering.

EPFs steer fascia matrix into wounds

To test whether matrix steering from fascia is caused by EPFs, we blocked fascia by implanting an impermeable dual surface expanded polytetrafluoroethylene (ePTFE) membrane[17] between the fascia and the PC in wounds of $En1^{Cre};R26^{VT2/GK3}$ mice (Fig. 4a, Methods). Surprisingly, wounds with implants remained completely open whereas sham controls closed within 21 days (Fig. 4b). After two months, EPFs trailed from the wound margins and under the membrane without generating scars (Fig. 4c, Extended Data Fig. 8a). Implants produced a transient inflammation that resolved even when the wound remained open. Two-month-old wounds with implants showed normal leukocyte and pro- and anti-inflammatory interleukins levels (Extended Data Fig. 8b–i), consistent with the clinical use of ePTFE as immunologically inert membranes. The coagulation cascade also was unaltered at the border between the dermis and the membrane (Extended Data Fig. 8j, k). These results indicate that the lack of scarring with ePTFE membranes does not reflect chronic inflammation or poor clotting, but rather a blockade of fascia steering mediated by the fascia

fibroblasts. These findings further support the notion that scar tissue is mostly derived from the fascia, since dermal EPFs or dermal matrix are unable to repair wounds in the absence of fascia movements.

Fig. 4

Fascia EPFs steer scar primordium into wounds.

a, 8-mm diameter ePTFE membranes were implanted between the skin and fascia in fresh 6-mm diameter wounds to block fascia steering. **b**, ePTFE-implanted or sham wound closure (left) determined from photographs (right) at specified time points. Individual values, n = 3 biological replicates. Unpaired two-tailed t-test, 95% CI. **c**, Sham (left) or ePTFE-implanted (right) wounds at 63 dpw. Trichrome staining (top) and collagen immunolabelling (middle). Magnifications (1, 2 (bottom)) show multiclonal dermal EPFs. Representative images from 3 biological replicates. **d**, Fascia tissue around fresh 5-mm diameter wounds was mechanically separated from the skin above using a metal paddle. **e**, Fascia-released or control wound closure (left) determined from photographs (right) at specified time points. Individual values, n = 8 (0–3 dpw), 6 (5 dpw), 4 (7 dpw) and 2 (10 dpw) images from 8 biological replicates. Unpaired two-tailed t-test, 95% CI. **f**, Trichrome-stained wounds at 3, 5 and 7 dpw from control or fascia-released wounds. Representative images from 8 biological replicates. **g**, Fascia cell depletion in $R26^{iDTR}$ neonates. **h**, Fluorescence image (left) and trichrome-stained wounds at 7 dpw in GFP- (middle) or Cre-transduced (right) fascia. Representative images from 3 biological replicates. **i**, Scar-length measurements. Data are mean ± s.e.m.; n = 4 and 8 sections from 3 biological replicates. Unpaired two-tailed t-test, 95% CI. **j**, Depletion of fascia EPFs in chimeric grafts with fascia matrix labelling. **k**, Immunolabelling for collagens, and fascia matrix in control (left) or DT-treated (right) grafts. Representative images from 3 biological replicates. **l**, Matrix-labelling coverage. Data are mean ± s.e.m.; n = 6 sections from 3 biological replicates. Unpaired two-tailed t-test, 95% CI. Dashed lines delimit the implant. Dotted lines delimit the wound. Arrowheads indicate the original injury. Arrow indicates remaining labelled fascia matrix in DT-treated grafts. Scale bars, 50 μm (**c** (1 and 2)), 200 μm (**h**), and 500 μm (**c** (main image), **f**, **h**, **k**).

AQ7

Source data

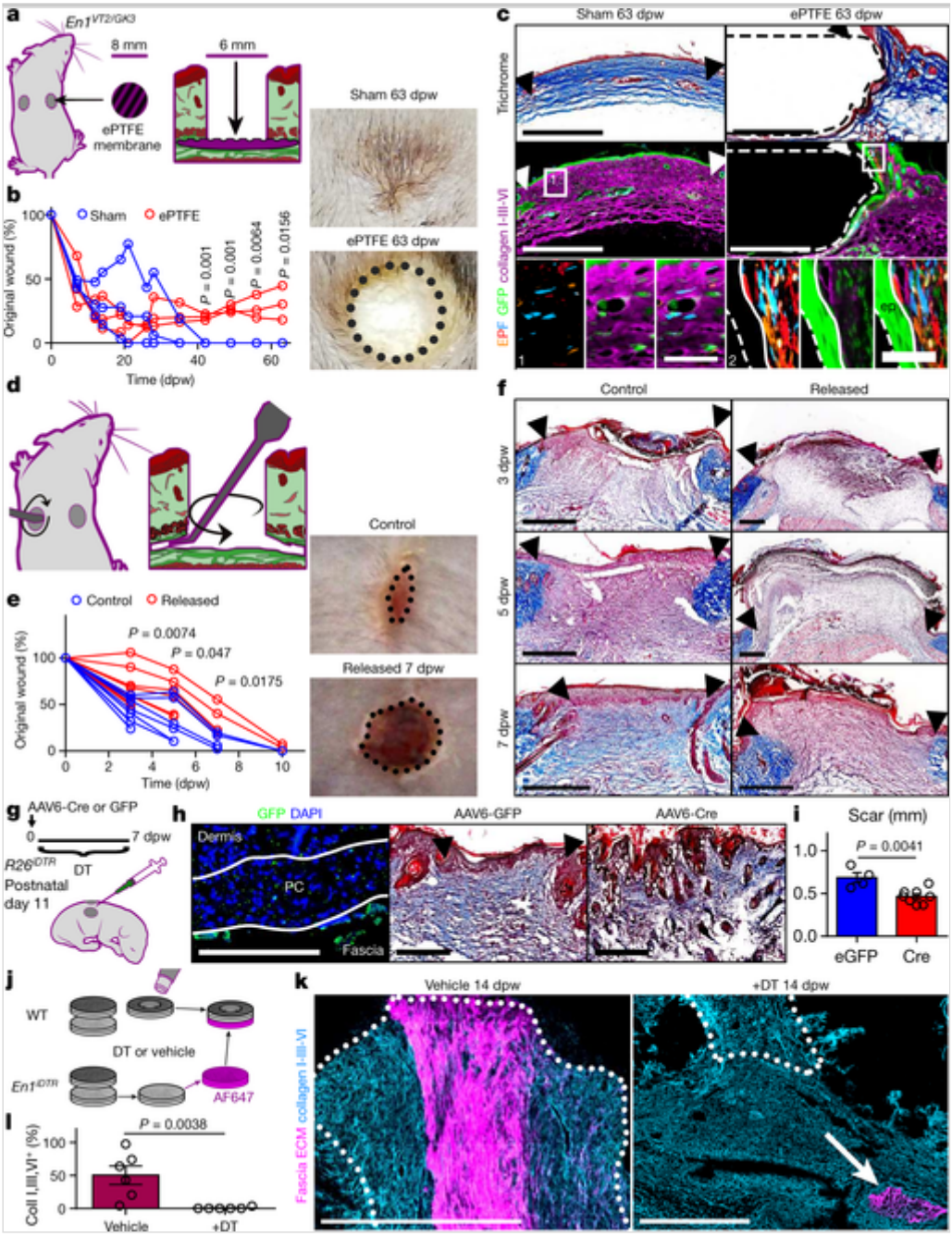

We next investigated whether mechanical separation between dermis and fascia alone, without barrier implants, would affect matrix steering and scar formation. To address this question, we performed full excisional wounds in wild-type mice and physically released the fascia below the PC around the wound (Fig. 4d). Wound closure from released-fascia wounds was significantly delayed, and wounds remained open early on, similarly to those documented following membrane implantations (Fig. 4e, f).

To definitively link fascia EPFs to matrix steering, we genetically ablated fascia EPFs using two separate strategies. First, we used a transgenic line that expresses the diphtheria toxin receptor (DTR) in a Cre-dependent manner ($R26^{iDTR}$), enabling us to deplete cells expressing Cre recombinase upon exposure to diphtheria toxin (DT). We thus generated Cre-expressing adeno-

associated viral particles (AAV6-Cre) and injected them into the fascia of $R26^{iDTR}$ pups underneath freshly made full excisional wounds (Fig. 4g). Scar size from AAV6-Cre transduced mice treated with DT were significantly smaller those from controls (Fig. 4h, i).

Second, we used $En1^{Cre}$;$R26^{iDTR}$ double transgenic mice, in which DTR expression is restricted to EPFs, making them susceptible to DT-mediated ablation. We corroborated the ablation of fascia EPFs in cultured biopsies 6 days after acute exposure to DT for 1 h. Effective dose of DT prevented the normal increase in collagen fibre density observed in control samples and decreased the cell density by 2.5 times (Extended Data Fig. 9a–c). Live imaging showed absence of any matrix steering after DT exposure (Extended Data Fig. 9d, e, Supplementary Video 6), confirming that fascia EPFs are essential for matrix steering.

Next, we created chimeric grafts using dermis from wild-type mice and fascia from $En1^{Cre}$;$R26^{iDTR}$ mice. We ablated fascia EPFs using DT and labelled the matrix before transplantation (Fig. 4j). Ablation of fascia EPFs prevented matrix steering into the wound (Fig. 4k, l) and instead labelled matrix remained in the fascia layer below. Together, our data demonstrate that fascia resident EPFs actively steer matrix to seal open wounds.

To check whether fibroblast proliferation preceded and was needed for matrix steering, we analysed the proliferation rate in our matrix-tracing experiments. Expansion of the fascia gel beneath the wound occurred during the first days after injury, whereas cell proliferation peaked after one week (Extended Data Fig. 10a–c), indicating that proliferation is not required for matrix steering. Furthermore, treatment with a proliferation inhibitor had no effect on fascia matrix steering in vitro (Extended Data Fig. 9f–k, Supplementary Video 7). Our results demonstrate that fascia matrix works as an expanding sealant that quickly clogs deep wounds independently of cell proliferation.

Fascia and keloid share marker signatures

Similar to mouse fascia matrix, human keloids present poorly structured and densely packed collagen fibres[18]. This motivated us to investigate the presence of fascia fibroblasts in keloid tissue. We screened for markers present in keloids and compared them with healthy dermis and the connective tissue in the subcutaneous space (fascia) of human skin across multiple anatomic locations (Fig. 5a, b). FAP and DPP4 were highly expressed in both fascia and keloids, with low expression in dermis. The fascia-restricted protein NOV was also prominently expressed in both human and mouse fascia, as well as in human

keloids and mouse scars (Fig. 5c–g). This preservation of fascia markers across mouse and human fascia and keloid scars suggests a common fascia origin for most human cutaneous scars.

Fig. 5

Marker signature in keloids and fascia.

a, **b**, Macroscopic images and trichrome staining of human back (**a**) and abdominal (**b**) skin showing fascia layers embedded in subcutaneous tissue. Arrows indicate the fascia. Representative images from 4 independent samples. **c**, Immunolabelling for DPP4, CD44 and FAP, and NOV and ACTA2 in fascia, dermis and keloids of human back skin. **d**, Relative fluorescence intensity (RFI) in **c**, normalized to the dermis. Data are mean ± s.e.m.; $n = 4$ images analysed from 4 biological replicates. One-way ANOVA with Tukey's test, 95% CI. **e**, **f**, Immunostaining for NOV in $En1^{Cre};R26^{mTmG}$ 14 dpw scars. **g**, Relative fluorescence intensity in **f**, normalized to the dermis. Data are mean ± s.e.m.; $n = 6$ images of 3 biological replicates. One-way ANOVA, Tukey's test, 95% CI. Dotted and broken lines delimit scar and fascia, respectively. Scale bars: 2 mm (**a**, **b**), 50 μm (**c**) and 200 μm (**e**, **f**).

Source data

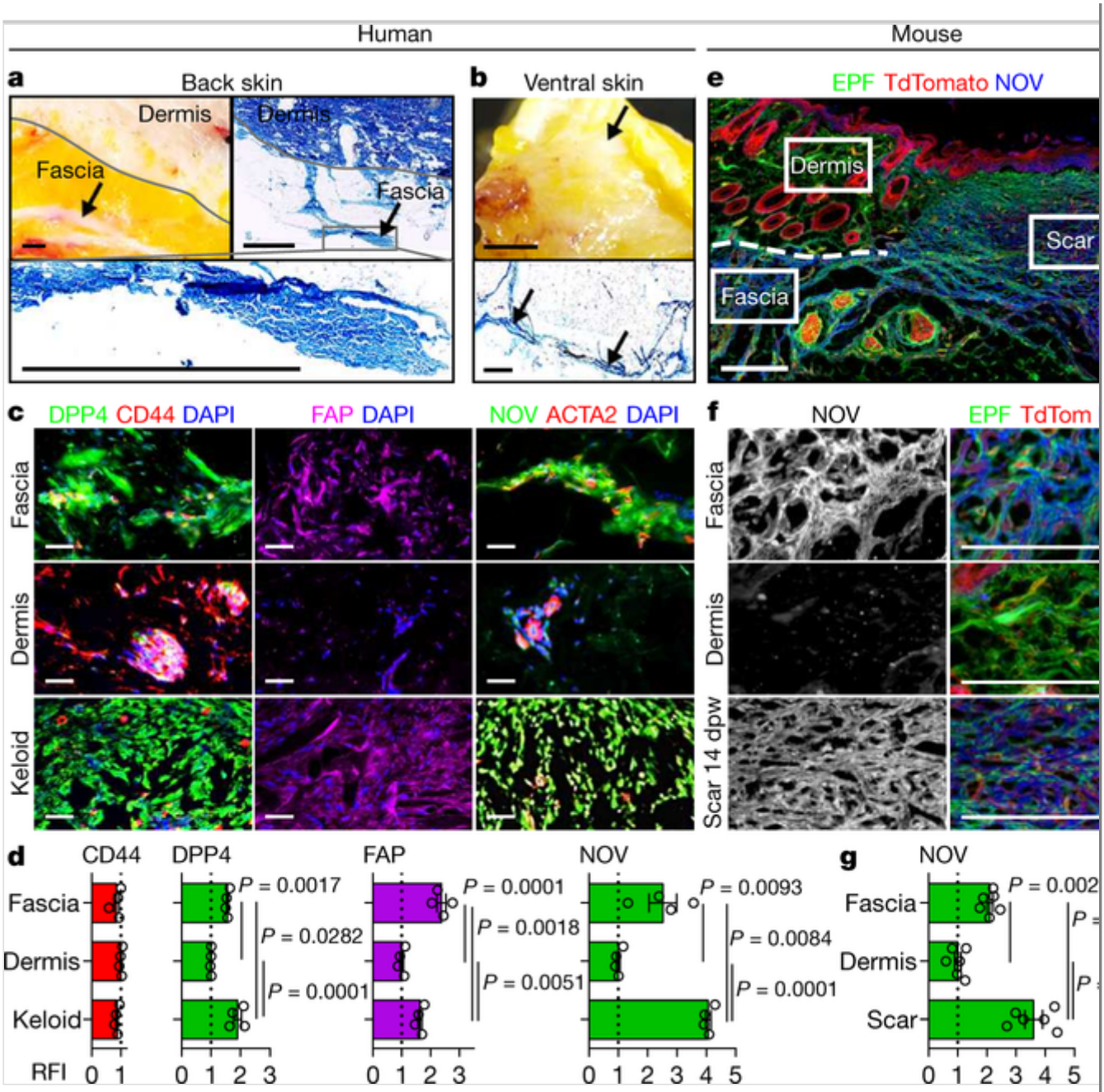

Discussion

Current models of wound healing propose that dermal fibroblasts migrate into wounds and locally deposit matrix de novo onto the granulation tissue provided by the coagulation cascade. This provisional matrix is then remodelled into a mature scar. On the basis of our findings in this study, we propose a revised model (Fig. 6) in which, in deep injuries, fascia fibroblasts pilot their local composite matrix into wounds that, in coordination with the coagulation cascade, form the provisional matrix. Thus, instead of de novo matrix deposition by dermal fibroblasts, a ‘scar primordium’ is steered by the fascia fibroblasts. Thus, fascia serves as an external store, or *externum repono*, of scar-forming provisional matrix, which represents an efficient mechanism to quickly seal large open wounds. Previous studies have shown that the matrix undergoes movement during early development and organ morphogenesis[19, 20, 21, 22].

To our knowledge, the extent and magnitude of matrix movements that we document here have not been observed during injury or regenerative settings. Cultured dermal fibroblasts have been shown to pull and reorient individual collagen or fibronectin fibres locally in cultured plates and in 3D in vitro assays[23, 24]. However, our findings reveal highly dynamic and large-scale movements of composite tissue matrix during injury that are mediated exclusively by specialized fibroblasts of the fascia.

Fig. 6

Revised wound healing model.

Superficial injuries heal by the classical fibroblast migration and de novo matrix deposition process. In response to a deep injury, fascia fibroblasts steer their surrounding tissue into wounds. Fascia-derived macrophages, endothelial and peripheral nerves rapidly clog the open wound. In coordination with the platelet response, the fascia matrix serves as a provisional matrix that undergoes remodelling until it forms a mature scar.

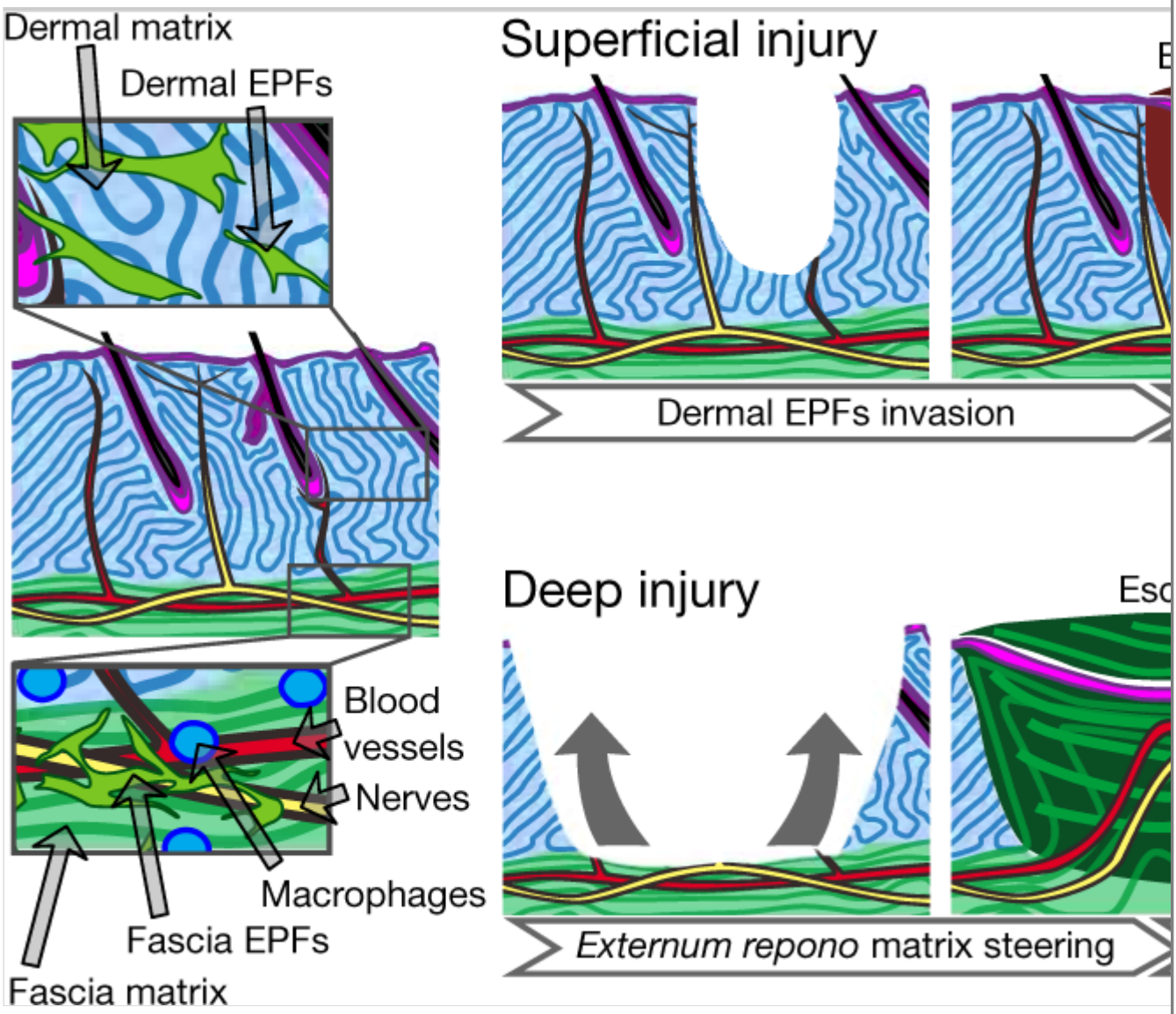

Our findings on the contribution of fascia to large scars and its blockage leading to chronic open wounds indicates that the spectrum of poor and excessive scarring in the skin, such as in diabetic and ulcerative wounds, as well as in hypertrophic and particularly keloid scars, might all be attributed to fascia. Indeed, the subcutaneous fascia varies widely according to species, sex, age and anatomic skin location[25]. In some mammals, the superficial fascia is loose, whereas in scar-prone species such as human, dog and horse, the superficial fascia is thicker. Human fascia further varies in thickness in different regions of the body[26]. For example, the lower chest, back, thigh and arm have much thicker and multi-layered membranous sheets, and it is these anatomic sites that are prone to form hypertrophic and keloid scars[27]. Understanding the topographic anatomy of the fascia layer may help explain scar phenotypes and severities, including the occurrences of hypertrophic and keloid scars.

Methods

Mice and genotyping

All mouse strains (C57BL/6J, *En1*^{Cre}, *R26*$^{VT2/GK3}$, *R26*^{mTmG}, *R26*^{iDTR}, *Rag2*$^{-/-}$ and Fox Chase SCID) were obtained from either Jackson laboratories, Charles River or generated at the Stanford University Research Animal Facility as described previously[12]. Animals were housed at the Helmholtz Center Animal Facility. Cages were maintained at constant temperature and humidity with a 12-h light cycle. Animals were supplied with food and water ad libitum. All animal experiments were reviewed and approved by the Government of Upper Bavaria and registered under the projects 55.2-1-54-2532-16-61 and 55.2-2532-02-19-23 and conducted under strict governmental and international guidelines. This study is compliant with all relevant ethical regulations regarding animal research. Unless specified, 8-to-10-week-old adult mice were used for the animal experiments. Both male and female mice were used. Cre-positive (Cre^{+}) animals from double-transgenic reporter mice were identified by detection of relevant fluorescence in the dorsal dermis. Genotyping was performed to distinguish mouse lines containing a 200-base pair (bp) *Cre* fragment (*Cre*$^{+/-}$) from the wild-type (*Cre*$^{-/-}$). Genomic DNA from the ear-clips was extracted using QuickExtract DNA extraction solution (Epicentre) following the manufacturer's guidelines. DNA extract (1 µl) was added to each 24 µl PCR. The reaction mixture was set up using Taq PCR core kit (Qiagen) containing 1 × coral buffer, 10mM dNTPs, 0.625units Taq polymerase, 0.5 µM forward primer ‘Cre_genotype_4F’ 5′-ATTGCTGTCACTTGGTCGTGGC-3′ (Sigma) and 0.5 µM reverse primer ‘Cre_genotype_4R’ 5′-GGAAAATGCTTCTGTCCGTTTGC-3′ (Sigma). PCRs were performed with initial denaturation for 10 min at 94 °C,

amplification for 30 cycles (denaturation for 30 s at 94 °C, hybridization for 30 s at 56 °C, and elongation for 30 s at 72 °C) and final elongation for 8 min at 72 °C, and then cooled to 4 °C. In every experiment, negative controls (non-template and extraction) and positive controls were included. The reactions were carried out in an Eppendorf master cycler. Reactions were analysed by gel electrophoresis.

Human skin samples

Fresh human skin and scar biopsies, from various anatomic locations, were collected from donors between 18–65 years of age, through the Section of Plastic and Aesthetic Surgery, Red Cross Hospital Munich (reference number 2018-157), and by the Department of Dermatology and Allergology, Klinikum rechts der Isar Technical University Munich (reference number 85/18S). Informed consent was obtained from all subjects before skin biopsies. Upon collection, these samples were directly processed for tissue culture or fixed with PFA and then processed for cryosection or paraffin section followed by histological or immunofluorescent analyses.

Fascia in vitro culture

Two in vitro systems were used. To visualize the changes in matrix architecture in real time, 2-mm-diameter biopsies were excised from P0 C57BL/6J neonates and processed for live imaging (SCAD assay, Patent Application no. PLA17A13). To determine the effectiveness of the DT treatment, muscle and fascia were manually separated from the rest of the skin in the chimeric grafts experiments and incubated with DT at different concentrations for 1 h at ambient temperature. Next, samples were washed with PBS and incubated in DMEM/F12 (Thermo Fisher) supplemented with 10% serum (Thermo Fisher), 1% penicillin–streptavidin (Thermo Fisher), 1% GlutaMAX (Thermo Fisher) and 1% non-essential amino acids solution (Thermo Fisher) in a 37 °C, 5% CO_2 incubator. Medium was routinely exchanged every other day. Samples were fixed at day 6 of culture with 2% paraformaldehyde and processed for histology.

Histology

Tissue samples were fixed overnight with 2% paraformaldehyde in PBS at 4 °C. Samples were rinsed three times with PBS, embedded in optimal cutting temperature (OCT, Sakura Finetek) and flash-frozen on dry ice. Six-micrometre sections were made in a Cryostar NX70 cryostat (Thermo fisher). Masson’s trichrome staining was performed with a Sigma-Aldrich trichrome stain kit, according to the manufacturer's guidelines. For immunolabelling, sections were air-dried for 5 min and fixed with −20 °C-chilled acetone for 20 min. Sections

were rinsed three times with PBS and blocked for 1 h at room temperature with 10% serum in PBS. Then, the sections were incubated with primary antibody in blocking solution for 3 h at ambient temperature. Sections were then rinsed three times with PBS and incubated with secondary antibody in blocking solution for 60 min at ambient temperature. Finally, sections were rinsed three times in PBS and mounted with fluorescent mounting media with 4,6-diamidino-2-phenylindole (DAPI). Primary antibodies used: goat-anti-ACTA2(αSMA) (1:50, Abcam), rabbit-anti-TUBB3 (1:100, Abcam), rat-anti-THY1(CD90) (1:100, Abcam), rat-anti-CD24 (1:50, BD biosciences), rabbit-anti-DPP4(CD26) (1:150, Abcam), rabbit-anti-PECAM1 (1:10, Abcam), rat-anti-CD34 (1:100, Abcam), rabbit-anti-COLLAGEN I (1:150, Rockland), rabbit-anti-COLLAGEN III (1:150, Abcam), rabbit-anti-COLLAGEN VI (1:150, Abcam), rabbit-anti-DLK1 (1:200, Abcam), rat-anti-ERTR7 (1:200, Abcam), rat-anti-F4/80 (1:400, Abcam), rabbit-anti-LYVE1 (1:100, Abcam), rat-anti-MOMA2 (1:100, Abcam), goat-anti-PDGFRα (1:50, R & D systems), rat-anti-LY6A(Sca1) (1:150, Biolegend), rat-anti-CD44 (1:100, Abcam), rabbit-anti-NOV/CCN3 (1:20, Elabscience), sheep-anti-FAP (1:100, R&D systems), rat-anti-IL12 (1:50, Biolegend), rat-anti-IL4 (1:50, Biolegend), rat-anti-CD19 (1:20, BD biosciences), hamster-anti-CD3e (1:100, Biolegend), rat-anti-NCR1 (1:20, Biolegend) and rat-anti-LY6G (1:100, Abcam). PacificBlue-, Alexa Fluor 488-, Alexa Fluor 568- or Alexa Fluor 647-conjugated antibodies (1:500, Life technologies) against suitable species were used as secondary antibodies.

Microscopy

Histological sections were imaged using a using a ZEISS AxioImager.Z2m (Carl Zeiss). For whole-mount 3D imaging of wounds, fixed samples were embedded in 35-mm glass bottom dishes (Ibidi) with low-melting point agarose (Biozym) and left to solidify for 30 min. Imaging was performed using a Leica SP8 multi photon microscope (Leica, Germany). For live imaging of fascia cultures, samples were embedded as just above. Attention was paid to mount the samples with the fascia facing up towards the objective. Imaging medium (DMEM/F-12; SiR-DNA 1:1,000) was then added. Time-lapse imaging was performed over 20 h under the multi-photon microscope. A modified incubation system, with heating and gas control (ibidi, catalogue nos. 10915 and 11922), was used to guarantee physiologic and stable conditions during imaging. Temperature control was set to 35 °C with 5% CO_2-supplemented air. Second harmonic generation signal and green auto-fluorescence as a reference were recorded every hour. 3D and 4D data was processed with Imaris 9.1.0 (Bitplane) and ImageJ (1.52i). Contrast and brightness were adjusted for better visibility.

Image analysis

Histological images were analysed using ImageJ. For quantification of labelled cells in our fate mapping experiments, we manually defined the wound, surrounding dermis, and adjacent fascia areas. We defined the wound as the area flanked by the near hair follicles on both sides, extending from the base of the epidermis down to the level of the hair follicles bulges. Surrounding dermis area was defined as the 200 μm immediately adjacent to the wound on both sides. Fascia area was defined as the tissue immediately below the wound. The number of labelled cells in each area was determined by quantifying the particles that were double-positive for DAPI and for the desired label (for example, DiI or GFP) channels. The coverage of the labelled matrix in the wound area was determined by quantifying the area that was double-positive for the labelled matrix and the collagen I-, III- and VI-staining signal. Cell density of $En1^{Cre};R26^{iDTR}$ cultures treated with DT was quantified by dividing the total cells (DAPI) by the matrix area (collagen I, III and VI), Collagens density was calculated as the collagens area coverage of the entire section area. Matrix movements in live-imaged cultures were determined by tracking the length of the two furthest points along the sample in both the SHG and auto-fluorescence channels. Length measurements were normalized to the original length at time 0. Wound size was normalized for each time point using the original area at day 0. Scar length was quantified from randomly selected sections taken from the middle of the scar using the two flanking hair follicles as a reference. RFI was calculated by measuring the mean grey value and normalize to the dermis images. Fractal analysis was performed using the ImageJ plug-in ‘FracLac’29 (FracLac2015Sep090313a9390) using the same settings and preprocessing as previously described[13].

DiI labelling of fascia in animals

Two 5-mm-diameter full-thickness excisional wounds were created on the back of 8- to 10-week-old C57BL6/J mice with a biopsy punch. Lipophilic Vybrant DiI dye (Life technologies, V22885) (10–20 μl) was injected into the exposed fascia directly above the dorsal muscles. Wounded tissue was harvested 14 dpw and processed for histology and imaging by fluorescence microscopy.

Chimeric skin transplantation

Full-thickness 6-mm-diameter biopsies were collected from the back-skin of either $R26^{mTmG}$, $R26^{VT2/GK3}$, $En1^{Cre};R26^{mTmG}$, $En1^{Cre};R26^{iDTR}$ or C57BL6/J adult mice. Using the PC muscle layer as an anatomical reference, the fascia together with the muscle layer were carefully separated from the dermis and epidermis using Dumont no. 5 forceps (Fine Science Tools) and a 26G needle under the fluorescent stereomicroscope (M205 FA, Leica). EPFs from

fascia + muscle samples of *En1*^{Cre};*R26*^{iDTR} mice were ablated by incubation with 20 µg ml^{-1} of diphtheria toxin (Sigma-Aldrich, D0564) or only DMEM/F12 as vehicle for 1 h at ambient temperature followed by 3 washing steps with PBS. At this point, the matrix samples were labelled by incubation with 100 µM Alexa Fluor NHS Ester (Life Technologies, A20006) or Pacific Blue succinimidyl ester (Thermo Fisher, P10163) in PBS for 1 h at ambient temperature followed by 3 washing steps with PBS. Chimeras were made by placing the epidermis + dermis portion of a mouse strain on top of the muscle + fascia of another strain and left to rest for 20 min at 4 °C inside a 35-mm culture dish with 2 ml of DMEM/F12. Special attention was paid on preserving the original order of the different layers (top to bottom: epidermis > dermis > muscle > fascia). Then, a 2 mm 'deep' full thickness was excised from the chimeric graft using a biopsy punch in the middle of the biopsy. To create 'superficial' wounds, the 2-mm excision was done only in the epidermis + dermis half before reconstitution with the bottom part. 'Wounded' chimeric grafts were then transplanted into freshly-made 4-mm-diameter full-thickness excisional wounds in the back of either *RAG2*$^{-/-}$ or Fox Chase SCID immunodeficient 8- to 10-week-old mice. Precautions were taken to clean out the host blood from the fresh wound before the transplant and to leave the graft to dry for at least 20 min before ending the anaesthesia, to increase the transplantation success. To prevent mice from removing the graft, a transparent dressing (Tegaderm, 3M) was placed on top of the grafts.

In situ matrix tracing and EdU pulses

Eight- to ten-week-old C57BL6/J mice received subcutaneous 20-µl injections of 10 mg ml^{-1} FITC NHS ester in physiological saline with 0.1 M sodium bicarbonate pH9 (46409, Life technologies) four and two days before wounding. At 2, 6 or 13 dpw, mice received 200 µl intraperitoneal injections of 1 mg ml^{-1} EdU in PBS. Samples were collected 24 h after the EdU pulse and processed for cryosection and imaging by fluorescence microscopy.

Flow cytometry

Fascia and dermis were physically separated from the back-skin of C57BL6/J or *En1*^{Cre};*R26*^{mTmG} mice under the fluorescence stereomicroscope as before. Harvested tissue was minced with surgical scissors and digested with an enzymatic cocktail containing 1 mg ml^{-1} collagenase IV, 0.5 mg ml^{-1} hyaluronidase, and 25 U ml^{-1} DNase I (Sigma-Aldrich) at 37 °C for 30 min. The resulted single cell suspension was filtered and incubated with conjugated/unconjugated primary antibodies (dilution 1:200) at 4 °C for 30 min, followed by an incubation with a suitable secondary antibody when needed at 4 °C for 30 min. Cells were washed and stained with Sytox blue dye (dilution

1:1,000. Life technologies, S34857) for dead cell exclusion. Cells were subjected to flow cytometric analysis using a FACSAria III (BD Bioscience). Fibroblasts were gated as the lineage negative (Lin^-) fraction not expressing the PTPRC, PECAM1, LY76, LYVE-1, or EPCAM markers. Primary antibodies used: anti-DLK1 (Abcam), anti-CD9 (Santa Cruz), anti-NGFR (Miltenyi), anti-F4/80 (Abcam), AlexaFluor790-anti-NG2 (Santa Cruz), FITC-anti-DPP4 (eBioscience), PerCP-eFluor710-anti-ITGB1 (eBioscience), anti-CD34 (Abcam), PerCP-Cy5.5-anti-CD24 (eBioscience), APC-Fire750-anti-CD34 (Biolegend), APC-anti-ITGA7 (R&D systems), PerCP-Cy5.5-anti-LY6A (eBioscience), PE-Vio770-anti-PDGFRα (Miltenyi), PerCP-Vio700-anti-CD146 (Miltenyi), APC-anti-PECAM1 (eBioscience), eFluor660-anti-LYVE1 (Thermo fisher), APC-LY76(TER119), APC-anti-EPCAM(CD326) and APC-anti-PTPRC. Secondary antibodies used: Alexa Fluor 488 goat anti-rabbit (Life technologies) and AlexaFluor568 goat anti-rat (Life technologies).

Scanning electron microscopy

Skin biopsies of adult C57BL6/J mice were collected, and the fascia was manually separated as before. Samples were then fixed overnight with paraformaldehyde and glutaraldehyde, 3% each, in 0.1% sodium cacodylate buffer pH 7.4 (Electron Microscopy Sciences). Samples were dehydrated in gradual ethanol and dried by the critical-point method, using CO2 as the transitional fluid (Polaron Critical Point Dryer CPC E3000; Quorum Technologies) and observed by scanning electron microscopy (JSM 6300F; JEOL).

ePTFE membrane implants

These membranes are routinely used in the clinic to circumvent post-operative adhesions after laparoscopic ventral incisional hernia repairs[17]. Two 6-mm-diameter full-thickness excisional wounds were created with a biopsy punch on the back of 8-week old $En1^{Cre}$;$R26^{VT2/GK3}$ or C57BL6/J mice. Sterile 8-mm-diameter ePTFE impermeable membranes (Dualmesh, GORE) were implanted between the surrounding skin and the fascia underneath, to cover the open wound on the right side. For this, the surrounding skin was loosen using Dumont no. 5 forceps and spatula (10090-13, Fine Science Tools). The dual-surface membrane was implanted with the attaching face facing out, so to promote dermal cell attachment, while the smooth surface was in direct contact with the fascia. The left sham control wound underwent the same procedure without implanting any membrane. Each wound was photographed at indicated time points, and wound areas were measured using ImageJ. Wound sizes at any given time point after wounding were expressed as percentage of initial (day 0) wound area. At 7 or 63 dpw, samples were collected and processed for histology.

Released fascia injury in adult mice

Two 5-mm-diameter full-thickness excisional wounds were created with a biopsy punch on the back of 8-week old male C57BL6/J mice. The skin around the wound on the left side was separated from the underneath skeletal muscle using a sterilized gold-plated 3 × 5 mm genepaddles (Harvard Apparatus, 45-0122) to release the fascia layer. The right wound served as a control. Each wound was digitally photographed at indicated time points, and wound areas were measured using Photoshop (Adobe Systems). Wound sizes at any given time point after wounding were expressed as percentage of initial (day 0) wound area. The harvested tissue at the indicated time points was processed for cryosection and Masson's trichrome staining for histology.

Viral particle production

AAV6 expressing GFP or Cre recombinase were produced by transfecting the AAVpro 293T Cell Line (Takara Bio, 632273) with pAAV-U6-sgRNA-CMV-GFP (Addgene, 8545142) or pAAV-CRE Recombinase vector (Takara Bio, 6654), pRC6 and pHelper plasmids procured from AAVpro Helper Free System (Takara Bio, 6651). Transfection was performed with PEI transfection reagent and viruses were harvested 72 h later and purified with an AAVpro purification kit (Takara Bio, 6666) and titre was calculated using real-time PCR.

Fascia cells ablation with AAV6-Cre viral particles and DT treatment in pups

Two 3-mm-diameter full-thickness excisional wounds were created with a biopsy punch on the back of postnatal day 11 (P11) $R26^{iDTR}$ mice. Twenty microlitres of Cre-expressing AAV6-Cre or control AAV6-eGFP at viral titre of 5×10^{11} ml^{-1} were injected subcutaneously at the area between the two wounds. DT solution at 1 ng μl^{-1} in PBS was intraperitoneally injected to each mouse once per day for 7 days at the dosage of 5 ng g^{-1}. Tissue was collected seven days after wounding.

Statistics

Statistical analyses were performed using GraphPad Prism software (v.6.0, GraphPad). Statistical test and *P* values are specified in the figure legends and in the corresponding plots. For simplicity, *P* values below 0.0001 were stated as equal to 0.0001.

Reporting summary

Further information on research design is available in the Nature Research Reporting Summary linked to this paper.

Online content

Any methods, additional references, Nature Research reporting summaries, source data, extended data, supplementary information, acknowledgements, peer review information; details of author contributions and competing interests; and statements of data and code availability are available at https://doi.org/10.1038/s41586-019-1794-y.

Extended data

is available for this paper at https://doi.org/10.1038/s41586-019-1794-y.

Supplementary information

is available for this paper at https://doi.org/10.1038/s41586-019-1794-y.

Publisher's note Springer Nature remains neutral with regard to jurisdictional claims in published maps and institutional affiliations.

Peer review information *Nature* thanks Christopher Buckley and the other, anonymous, reviewer(s) for their contribution to the peer review of this work.

Acknowledgements

We thank G. Mettenleiter for technical assistance with the SEM; S. Dietzel and the Core Facility Bioimaging at the Biomedical Centre of the Ludwig-Maximilians-Universität München for access and support with the multi-photon system. Y.R. was supported by the Human Frontier Science Program Career Development Award (CDA00017/2016), the German Research Foundation (RI 2787/1-1 AOBJ: 628819), the Fritz–Thyssen–Stiftung (2016-01277) and the European Research Council Consolidator Grant (ERC-CoG 819933). D.C.-G. was supported by the Consejo Nacional de Ciencia y Tecnología (CONACYT) and the Deutscher Akademischer Austauschdienst (DAAD).

Author contributions

Y.R. outlined and supervised the research narrative and experimental design. D.C.-G. performed the cell and matrix tracing experiments, chimeric skin transplantations ePTFE implantations and image analysis. D.J. performed the cell depletion with DT in pups, flow cytometry experiments and analysis, fascia release experiments and experiments with human skin samples. S.C. performed the live imaging and analysis. S.C. and P.R. performed 3D imaging and analysis.

H.Y. performed histology and immunofluorescence staining of human samples. J. W. provided veterinary advice and prepared animal experiment protocols. S.K.G. made the viral particles and performed titre quantification. Q.Y. assisted in the flow cytometry experiments. U.M. and T.V. collected consent from patients and the primary human tissue samples, and assisted with translational and clinical advice. U.M. wrote, in part, the ethical application for collection and use of human samples. M.A. and A.W. performed the scanning electron microscopy images. Y.R., D.C.-G. and D.J. wrote the manuscript.

Data availability

Source data for Figs. 1–5 and Extended Data Figs. 1–10 are provided with the paper. Additional information is available from the corresponding author on reasonable request.

Competing interests The authors declare no competing interests.

Extended data figures and tables

Extended Data Fig. 1

Fate mapping of fascia cells with DiI.

a, DiI labelling of fascia cells. **b**, Histology showing DiI^+ cells in uninjured controls (left) and at 14 dpw (right). Representative images of five biological replicates. **c**, Immunolabelling (top) and fractions (bottom) of DiI-positive cells expressing mesenchymal/fibroblast markers ITGB1, ER-TR7, THY1 and PDGFRα. Data are mean ± s.e.m.; n = 4 (5 in ITGB1) images analysed from 3 biological replicates. **d**, Immunolabelling (top) and fractions (bottom) of DiI-positive monocytes/macrophages (MOMA-2), lymphatic cells (LYVE1), endothelial cells (PECAM1) and nerve cells (TUBB3). Data are mean ± s.e.m.; n = 5 images analysed from 3 biological replicates. Lines delimit PC. The dotted line delimits the wound. Scale bars, 200 μm.
Source data

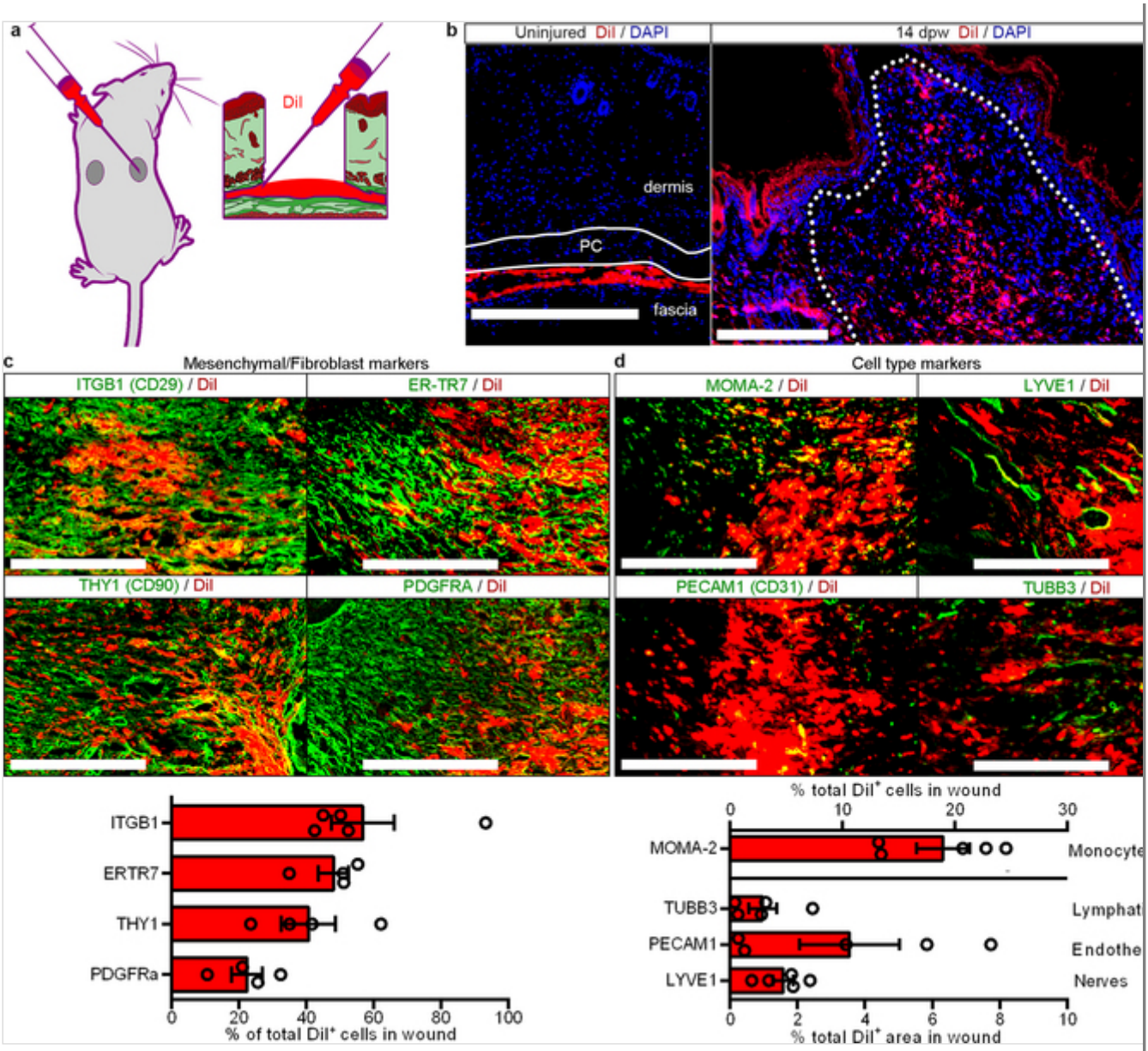

Extended Data Fig. 2

Fascia EPFs traverse PC.

a, Gating strategy for fibroblasts analysis. **b**, Percentages of fibroblasts (Lin^-) and lineage-positive cells in fascia and dermis. Data are mean ± s.e.m.; n = 4 independent experiments. Unpaired two-tailed t-test, 95% CI. **c**, Scatter plots of EPFs (GFP^+Lin^-) and ENFs ($TdTomato^+Lin^-$) in fascia and dermis. Representative plots of three independent experiments. **d**, EPF and ENF fractions in fascia and dermis. Data are mean ± s.e.m.; n = 4 independent experiments. Two-way ANOVA, multiple comparison Tukey's test, 95% CI. **e**, Endothelial cell ($PECAM1^+$), lymphatic cell ($LYVE1^+$), macrophages ($F4/80^+$) and nerve cell ($NGFR^+$) fractions in fascia and dermis. Data are mean ± s.e.m.; n = 3 biological replicates. Two-way ANOVA, multiple comparison Tukey's test, 95% CI. **f**–**k**, Representative images of 3D-rendered $En1^{Cre};R26^{mTmG}$ or $En1^{Cre};R26^{VT2/Gk3}$ back skin fascia from at least three biological replicates. **f**, Lateral view (left) and cross-

sections (right) of adult fascia. **g**, Top view (ventral side up) of neonate back skin. **h**, Top side view (top) and lateral cross-section (bottom) at the forelimb junction showing EPF traversing the PC. **i**, Top view at a muscle breach showing EPFs in both locations. **j**, Top view at a muscle opening where nerves pass through and polyclones of EPFs reside. **k**, Top view (top, epidermis side up) and lateral cross-section (bottom) of an adult superficial wound (3 dpw). Brocken lines delimit PC. Dotted lines delimit the epidermis. Scale bars, 1,500 μm (**g**), 100 μm (**f**, **i**, **j**) and 500 μm (**k**); v, vessels; nb, nerve bundles.

Source data

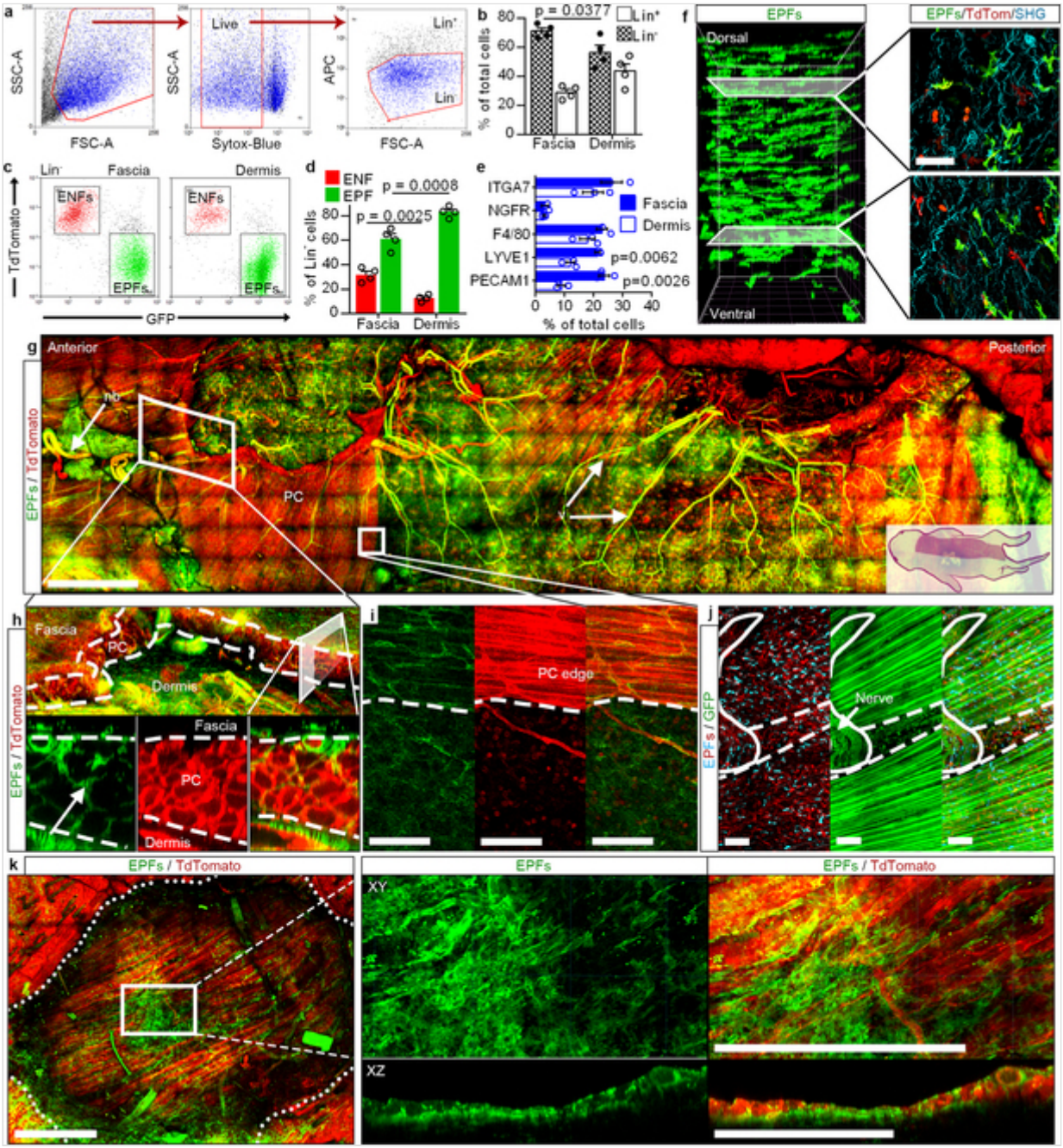

Extended Data Fig. 3

Fascia EPFs maintain position in steady conditions and recede from wounds over time.

a, Dermal versus fascia EPFs chimeras in uninjured conditions. **b**, Fascia (left) or dermal (right) EPFs-traced chimeras. Representative images of 3 biological replicates. **c**, Scars at 70 dpw from deep injuries of fascia EPF-traced chimeras immunolabelled for DPP4. Representative images of 3 biological replicates. **d**, Cleaved CASP3 expression in wounds from fascia (left) or dermal (right) EPF-traced chimeras from deep (top) or superficial (bottom) injuries at 14 dpw. **e**, Fractions of fascia or dermal EPFs in the wound, dermis or fascia control regions positive for cleaved CASP3. Data are mean ± s.e.m.; n = 6 and 5 (fascia and dermal EPF, respectively) images analysed from 5 biological replicates. Lines delimit the border between fascia and dermis. Dotted lines delimit the wound or scar. Scale bars, 200 μm.

Source data

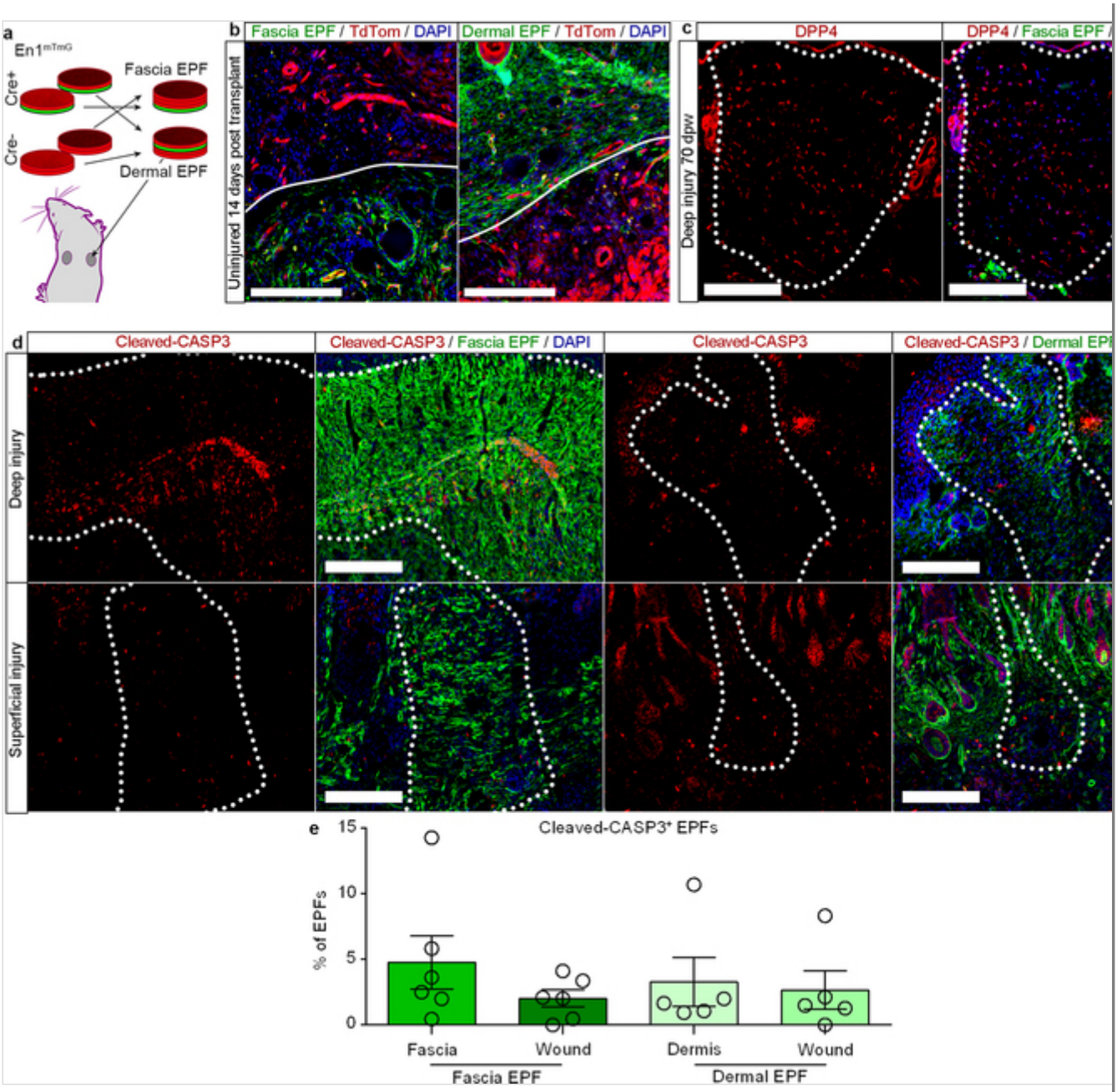

Extended Data Fig. 4

Fascia EPFs express wound fibroblast markers.

a, Dermal versus fascia EPF-traced chimeras with two injury conditions. **b**–**f**, Representative immunolabelling for the fibroblast markers DPP4 (**b**), DLK1 (**c**), CD24 (**d**), CD34 (**e**) and LY6A (**f**) from 4 biological replicates. **g**, Areas analysed (top) for marker-positive EPF quantification (bottom). Data are mean ± s.e.m.; $n = 4$ (DPP4 in dermal EPFs), 5 (all markers in dermal EPFs with the exception of DPP4 and all markers in fascia EPFs with the exception of DLK1, CD34 and LY6A), 6 (DLK1 in fascia EPFs), 7 (CD34 in fascia EPFs) or 11 (LY6A in fascia EPFs) images analysed from 4 biological replicates. One-way ANOVA, multiple comparison Tukey's test, 95% CI. Dotted lines delimit the wound bed. Scale bars, 200 μm.

Source data

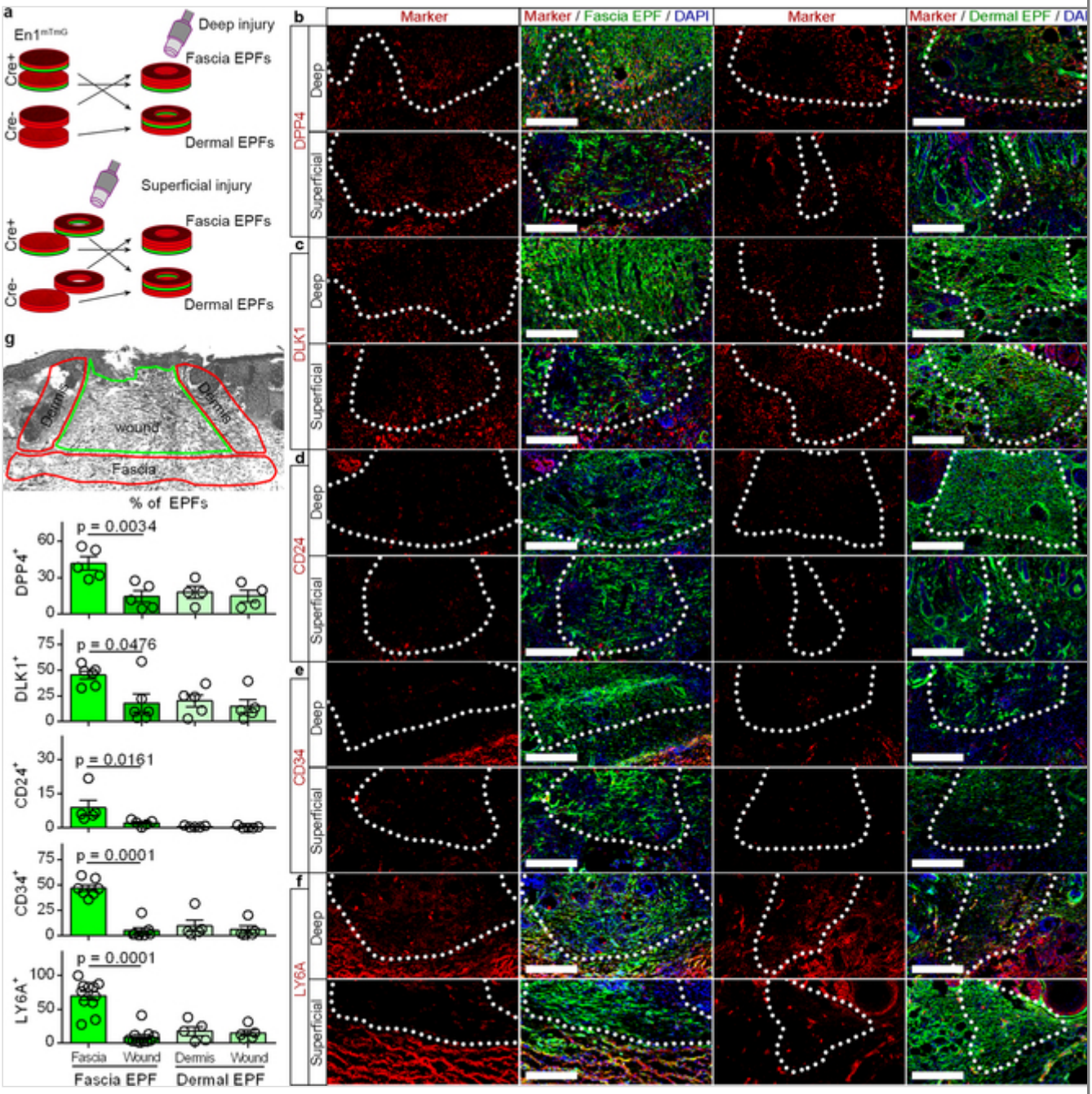

Extended Data Fig. 5

Differential expression of classical markers on fascia and dermal fibroblasts.

a, Gating strategy for fibroblast (Lin^-) cytometry. **b**, Histogram plots of fibroblast-marker expression in fascia or dermis derived fibroblasts from three biological replicates. **c**, Fraction of marker-positive cells from total fibroblast population. Data are mean ± s.e.m.; $n = 3$ biological replicates. Unpaired two-tailed *t*-test, 95% CI. **d**, Gating strategy for fascia EPF (Lin^- GFP^+) sorting and detection of LY6A,

PDGFR1, DPP4 and ITGB1 expression. Representative plots of three biological replicates.

Source data

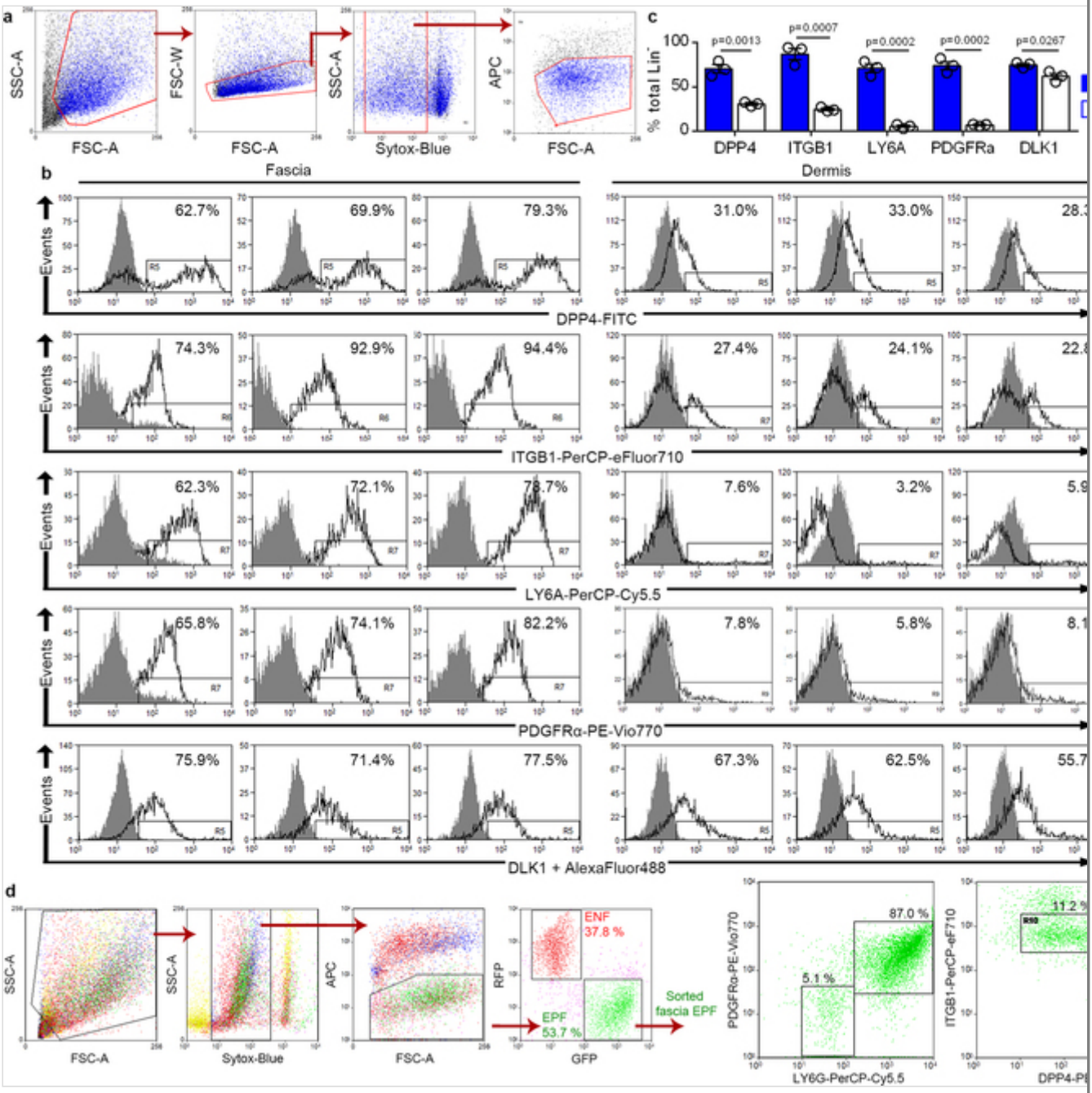

Extended Data Fig. 6

Fascia but not dermal matrix steers into wounds.

a, Matrix tracing in chimeric grafts. **b**, Grafts at 7 dpw immunolabelled for collagen I, III and VI. Representative image of three biological replicates. **c**, Label coverage fraction from total collagens in the wound at defined time points. Data are mean ± s.e.m.; n = 4 (7 dpw) and 9 (14 dpw) sections analysed from 3 biological replicates. Unpaired two-tailed t-test, 95% CI. **d**, Wounds at 14 dpw

immunolabelled for collagens. Representative images of three biological replicates. **e**–**f**, Higher magnification of the insets in **d**. **g**, **h**, Double matrix tracing in deep-injured dermal EPF-traced grafts at 7 dpw. Representative image of three biological replicates. **i**, **j**, Double matrix tracing in deep-injured fascia EPF-traced grafts at 14 dpw. Representative image of three biological replicates. **k**, **l**, Double matrix labelling in superficial-injured dermal EPF-traced grafts at 14 dpw immunolabelled for collagens. Representative image of three biological replicates. Dotted lines delimit the wound. Arrowheads mark the original injury. Continuous lines delimit the epidermis dermis margin. Scale bars, 500 µm (**b**), 100 µm (**d**–**f**) and 200 µm (**h**, **j**, **l**).

Source data

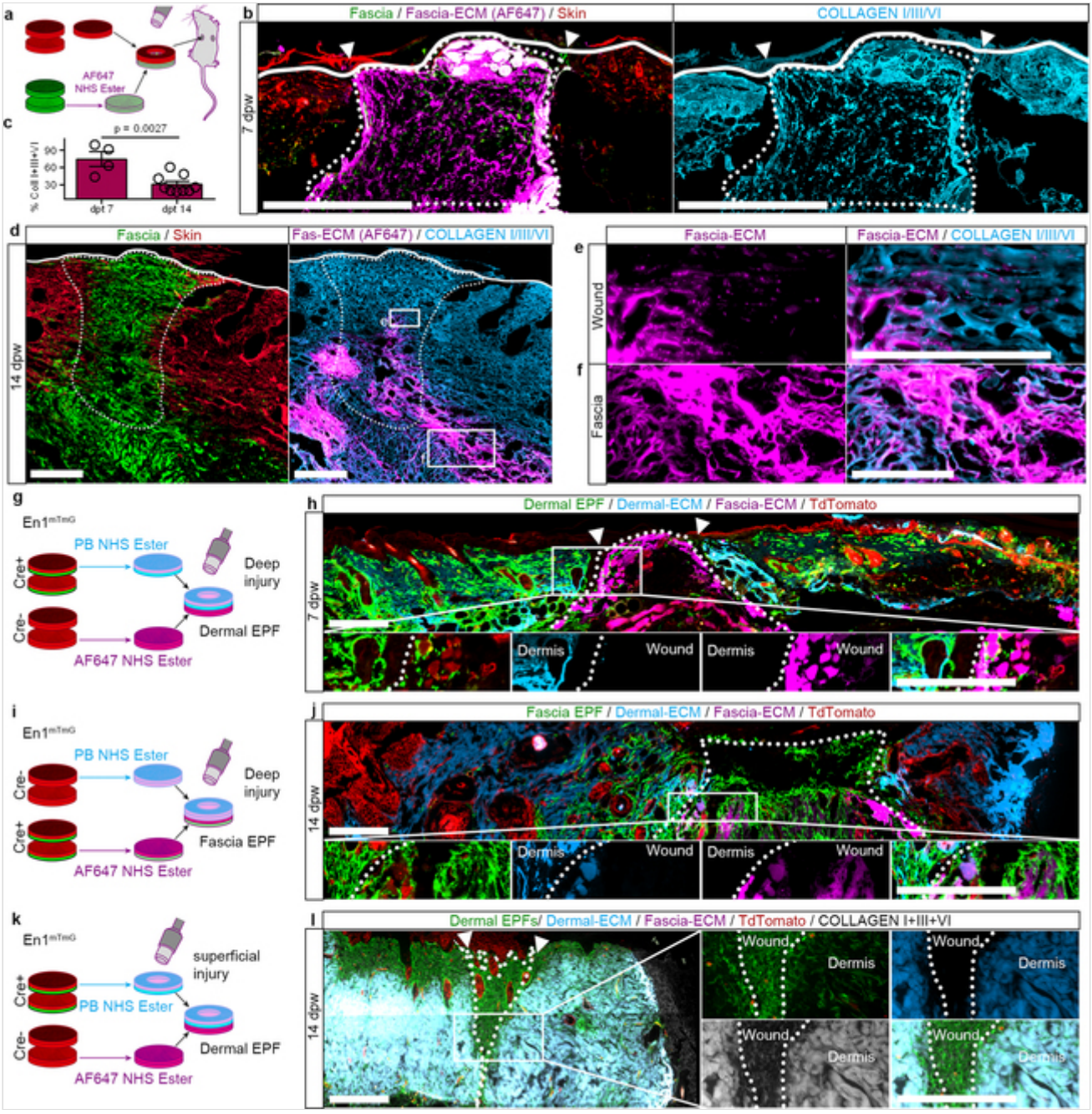

Extended Data Fig. 7

Fascia matrix forms the eschar and is remodelled in the wound.

a, Left, in situ matrix tracing and collagen I, III and VI immunolabelling at defined time points after wounding. Representative images of three biological replicates. Right, subsampled fractal dimension maps of the FITC signal of uninjured tissue and at 3 and 7 dpw, and the collagen signal at 14 dpw. **b**, Matrix label coverage from total collagen I, III and VI signal in the wound. Data are mean ± s.e.m.; $n = 3$ (uninjured), 4 (3 dpw), 7 (7 dpw) and 4 (14 dpw) sections analysed from 3 biological replicates. One-way ANOVA, Tukey's multiple comparisons. **c**, **d**, Average fractal dimension (**c**) and lacunarity (**d**) from subsampled maps. Data are mean ± s.e.m.; $n = 5$ (uninjured), 5 (3 dpw), 8 (7 dpw) and 3 (14 dpw) images analysed from 3 biological replicates. One-way ANOVA, Tukey's test, 95% CI. **e**, Scatter plot of average fractal dimension and lacunarity values. **f**, In situ matrix tracing and SELP immunolabelling at defined time points after wounding. Representative images of three biological replicates. The broken line separates dermis from fascia. Dotted lines indicate the wound. Scale bars, 200 μm.
Source data

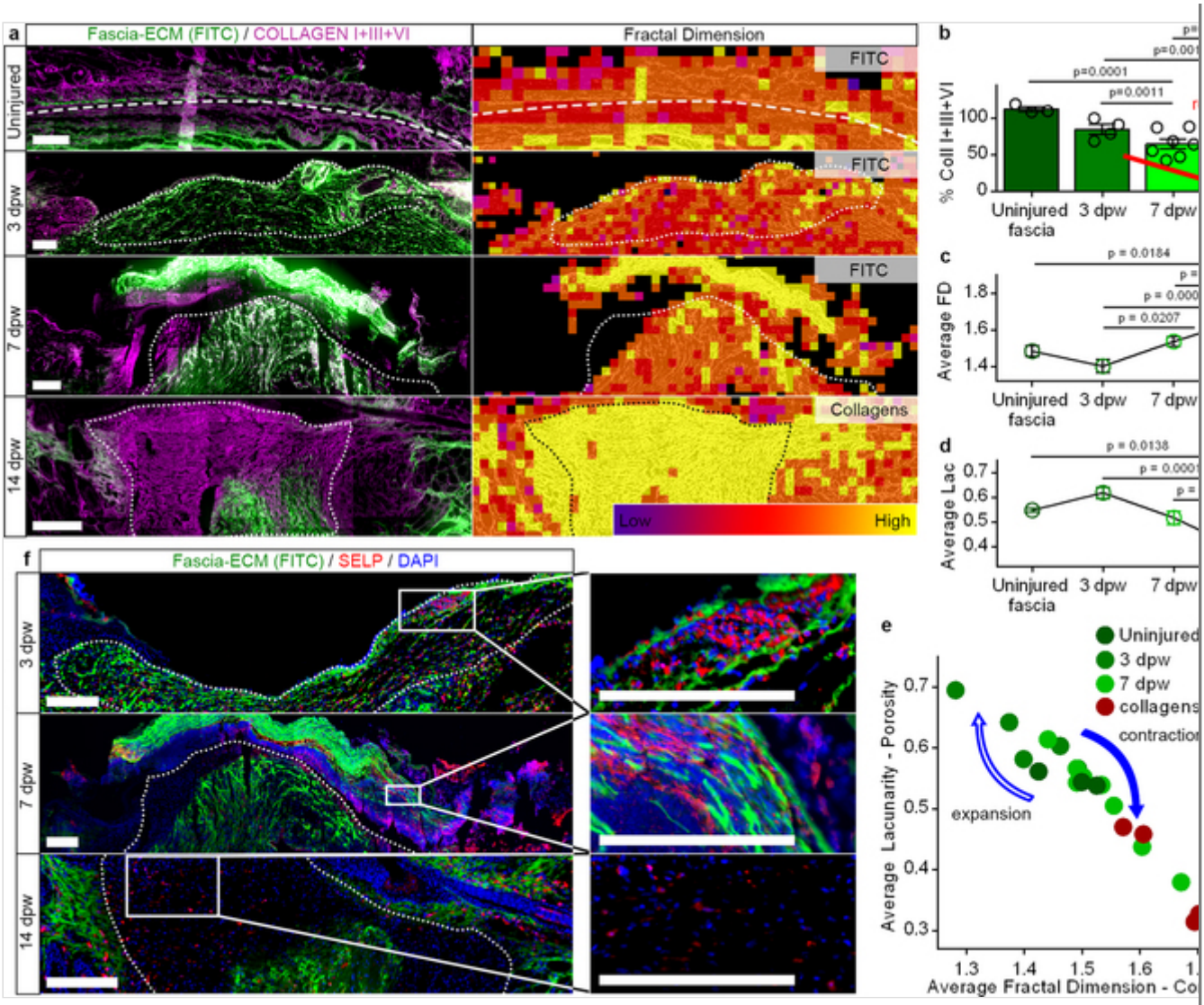

Extended Data Fig. 8

Inflammation resolution and coagulation stay unaffected during fascia blocking.

a, Sham (left) or ePTFE-implanted (right) wounds at 7 (top) or 63 dpw (bottom) immunolabelled for collagen I, III and VI. Representative images of three biological replicates. **b**–**i**, Immunolabellings (left) and fractions (right) of immune cells (PTPRC^{+}; **b**), neutrophils (LY6G^{+}; **c**), T cells (CD3^{+}; **d**), NK cells (NCR1^{+}; **e**), B cells (CD19^{+}; **f**), macrophages and monocytes (MOMA2^{+}; **g**) and cells expressing the pro- and anti-inflammatory cytokines (IL12 (**h**) and IL4 (**i**)). Mean with SEM, n = 3 images analysed from 3 biological replicates. Unpaired two-tailed t-test, 95% CI (b). One-way ANOVA, Tukey's test, 95% CI (c-i). **j**, Activated platelets (SELP) in 7 dpw sham and ePTFE-implanted wounds. Representative images of 3 biological replicates. **k**, Mean grey value of SELP signal. Data are mean ± s.e.m.; n = 3 images analysed from 3 biological replicates. Two-tailed Student's t-test, 95% CI. Dotted lines delimit the wound area. Scale bars, 200 µm (main images) and 100 µm (magnified insets).

Source data

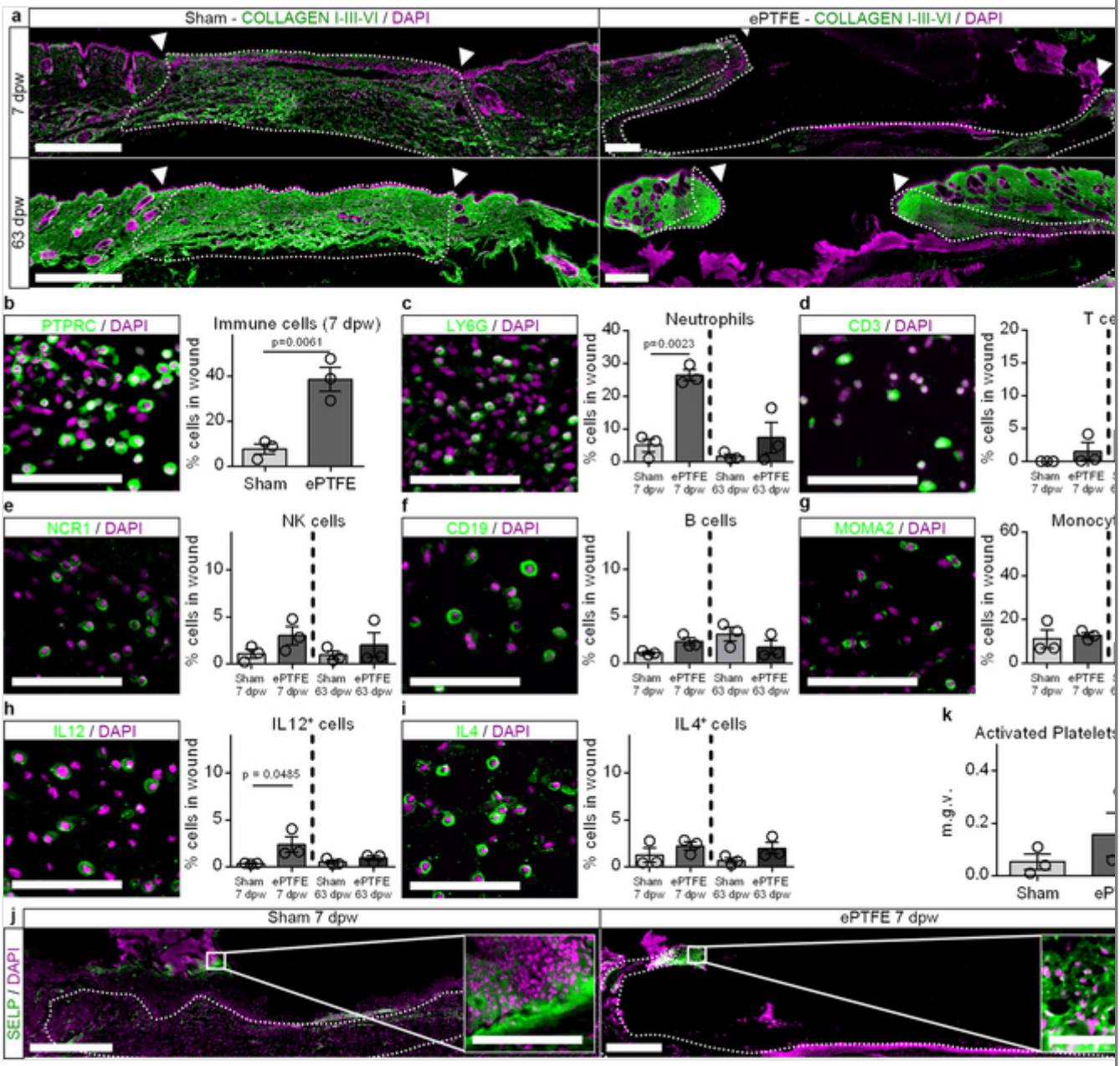

Extended Data Fig. 9

EPFs steer matrix in vitro independently of proliferation.

a, *En1*^{Cre};*R26*^{iDTR} biopsies at day 0 and 6 after short treatment with DT or vehicle, immunolabelled for collagen I, III and VI. Representative images of three replicates. **b**, Collagens density. Data are mean ± s.e.m.; *n* = 3 images analysed from 3 biological replicates. Two-way ANOVA, multiple comparison Tukey's test, 95% CI. **c**, Cell density. Data are mean ± s.e.m.; *n* = 3 images analysed from 3 biological replicates. One-way ANOVA, multiple comparison Tukey's test, 95% CI. **d**, **e**, Time-lapse images (**d**) and contraction rate (**e**) of *En1*^{Cre};*R26*^{iDTR} neonate fascia biopsy in culture treated with DT for 1 h. Representative samples from three

replicates. Contraction values obtained from Supplementary Videos 4, 6. **f**, Fascia biopsies treated with etoposide and immunolabelled for MKI67. **g**, Fraction of MKI67^{+} cells. Data are mean ± s.e.m.; n = 3 images analysed from 3 biological replicates. One-way ANOVA, Dunnett's multiple comparisons, 95% CI. **h**, **i**, Time-lapse images (**h**) and contraction rate (**i**) of neonate fascia biopsy in culture treated with 100 µM etoposide. Representative samples from three replicates. Contraction values obtained from Supplementary Videos 4, 7. **j**, Mean (± s.e.m.) matrix contraction velocity during the first 25 h of imaging; n = 25 values from Supplementary Video 7. Two-tailed Student's t-test, 95% CI. Lines show the distance between two tracked points in the SHG channel. Scale bars, 50 µm (**f**), 200 µm (**a**, **h**) and 500 µm (**d**).

Source data

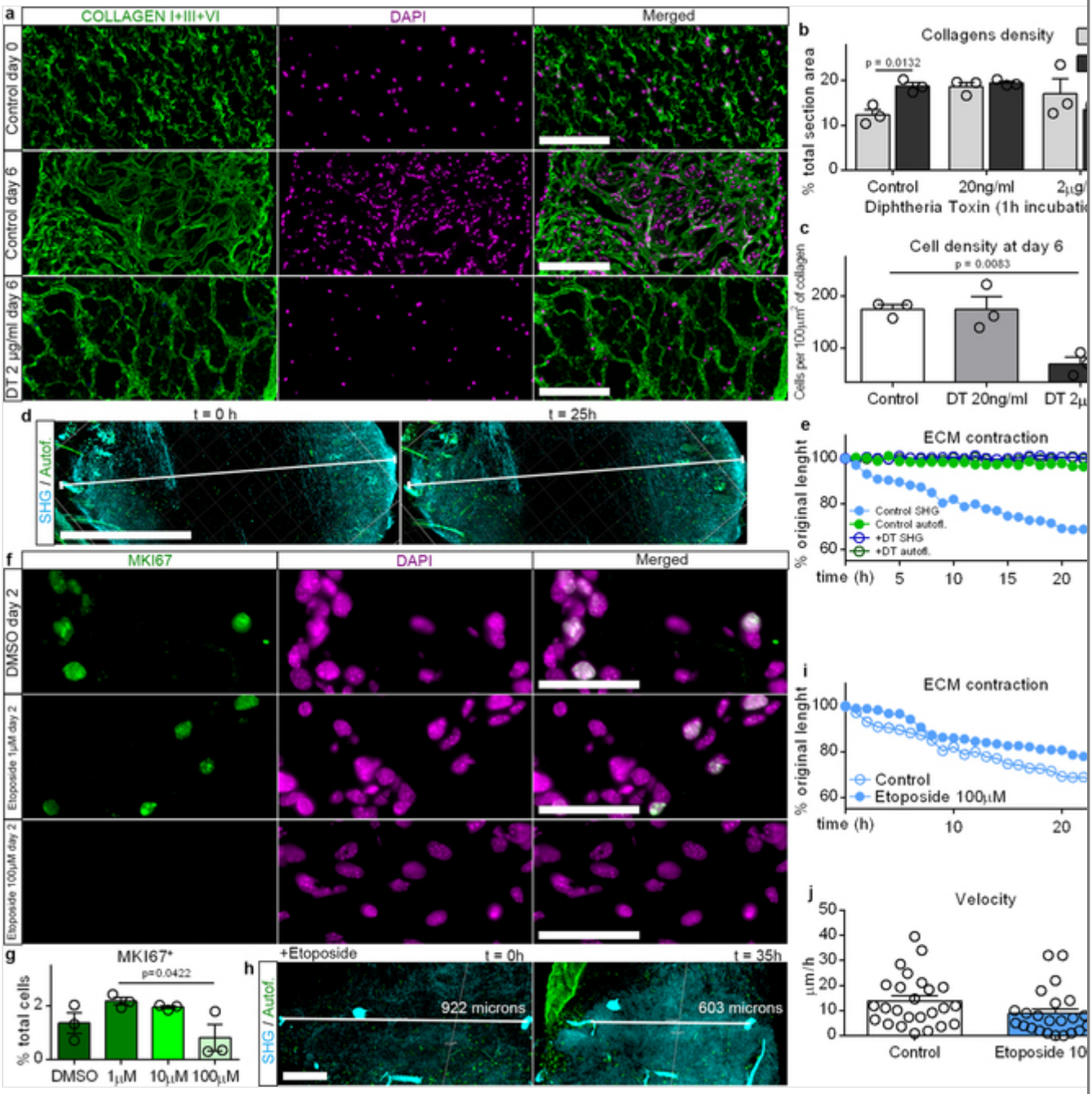

Extended Data Fig. 10

Fascia matrix steering precedes proliferation in vivo.

a, In situ fascia matrix labelling and EdU pulses. **b**, EdU detection in sections at defined time points. **c**, Fraction of EdU^+ cells in the wound from total EdU^+ cells. Data are mean ± s.e.m.; n = 3 (uninjured), 4 (3 dpw), 6 (7 dpw) and 4 (14 dpw) images analysed from 3 biological replicates. One-way ANOVA, Tukey's multiple comparisons. Arrows indicate EdU-positive nuclei. Arrowheads indicate the original injury site. Broken and dotted lines delimit fascia and wounds respectively. Scale bars, 200 µm.

Source data

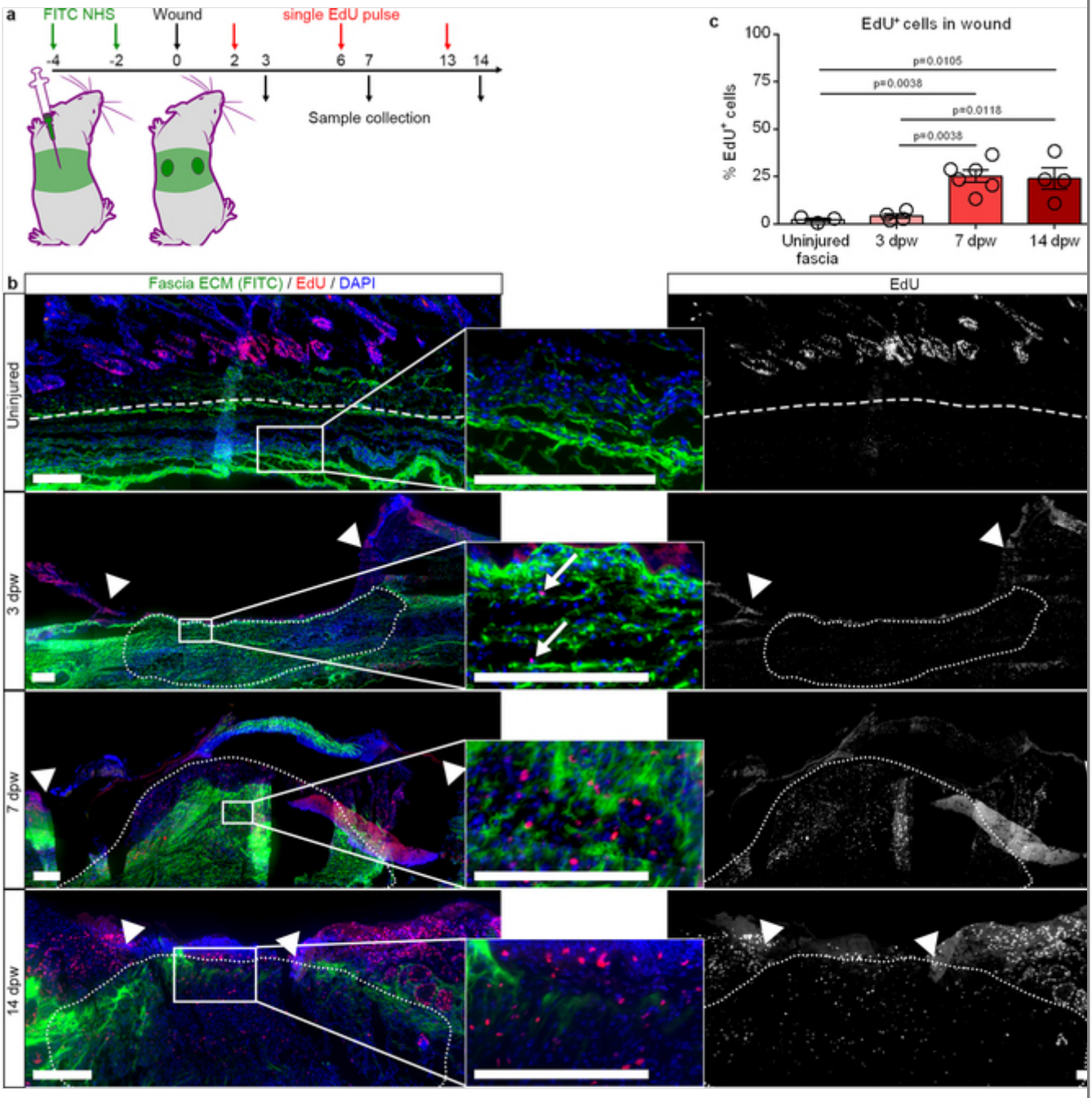

Supplementary information

Reporting Summary

Video 1

: 3D reconstruction of adult En1Cre;R26mTmG fascia. EPFs in green and SHG in cyan

Video 2

: 3D reconstruction of neonate En1Cre;R26mTmG back-skin and fascia. EPFs in green and TdTomato in red. Anterior-to-posterior axis from top to bottom of the video frame. Mid-to-lateral axis from left to right of the video frame

Video 3

: 3D reconstruction of adult En1Cre;R26mTmG back-skin wound 3 dpw. EPFs in green, TdTomato in red, SHG in cyan, and COLLAGEN I in magenta

Video 4

: Time-lapse of 3D rendered P0 C57BL6/J fascia biopsy in culture. Second harmonic generation (SHG) in cyan and autofluorescence in green

Video 5

: 3D reconstruction of day 14 wounds after transplantation of chimeric grafts with labeled matrix. TdTomato (Skin) in red, GFP (Fascia) in green, NHS AF647 in magenta, and COLLAGEN I+III+VI immunolabeling in blue. Skin to fascia orientation from top to bottom of the video frame

Video 6

: Time-lapse of 3D rendered P0 En1Cre;R26iDTR fascia biopsy in culture treated with an acute exposure of 2 μg/ml of diphtheria toxin. Second harmonic generation (SHG) in cyan and autofluorescence in green

Video 7

: Time-lapse of 3D rendered P0 C57BL6/J fascia biopsy in culture treated with 100 μM etoposide. Second harmonic generation (SHG) in cyan and autofluorescence in green

Source data

Source Data Fig. 1 Source Data Fig. 2 Source Data Fig. 3 Source Data Fig. 4

Source Data Fig. 5 Source Data Extended Data Fig. 1

Source Data Extended Data Fig. 2 Source Data Extended Data Fig. 3

Source Data Extended Data Fig. 4 Source Data Extended Data Fig. 5

Source Data Extended Data Fig. 6 Source Data Extended Data Fig. 7

Source Data Extended Data Fig. 8 Source Data Extended Data Fig. 9

Source Data Extended Data Fig. 10

References

1. Marshall, C. D. et al. Cutaneous scarring: basic science, current treatments, and future directions. *Adv. Wound Care* **7**, 29–45 (2018).

2. Finnerty, C. C. et al. Hypertrophic scarring: the greatest unmet challenge after burn injury. *Lancet* **388**, 1427–1436 (2016).

3. Morton, L. M. & Phillips, T. J. Wound healing and treating wounds: differential diagnosis and evaluation of chronic wounds. *J. Am. Acad. Dermatol*. **74**, 589–605, quiz 605–606 (2016).

4. Do, N. N. & Eming, S. A. Skin fibrosis: models and mechanisms. *Curr. Res. Transl. Med*. **64**, 185–193 (2016).

5. Sen, C. K. et al. Human skin wounds: a major and snowballing threat to public health and the economy. *Wound Repair Regen*. **17**, 763–771 (2009).

6. Hinz, B. Myofibroblasts. *Exp. Eye Res*. **142**, 56–70 (2016).

7. Driskell, R. R. et al. Distinct fibroblast lineages determine dermal architecture in skin development and repair. *Nature* **504**, 277–281 (2013).

8. Greenhalgh, S. N., Conroy, K. P. & Henderson, N. C. Healing scars: targeting pericytes to treat fibrosis. *QJM* **108**, 3–7 (2015).

9. Plikus, M. V. et al. Regeneration of fat cells from myofibroblasts during wound healing. *Science* **355**, 748–752 (2017).

10. Shook, B. A. et al. Myofibroblast proliferation and heterogeneity are supported by macrophages during skin repair. *Science* **362**, eaar2971 (2018).

11. Mori, L., Bellini, A., Stacey, M. A., Schmidt, M. & Mattoli, S. Fibrocytes contribute to the myofibroblast population in wounded skin and originate from the bone marrow. *Exp. Cell Res*. **304**, 81–90 (2005).

12. Rinkevich, Y. et al. Identification and isolation of a dermal lineage with intrinsic fibrogenic potential. *Science* **348**, aaa2151 (2015).

13. Jiang, D. et al. Two succeeding fibroblastic lineages drive dermal development and the transition from regeneration to scarring. *Nat. Cell Biol*. **20**, 422–431 (2018).

14. Adstrum, S., Hedley, G., Schleip, R., Stecco, C. & Yucesoy, C. A. Defining the fascial system. *J. Bodyw. Mov. Ther*. **21**, 173–177 (2017).

15. Stecco, C. & Schleip, R. A fascia and the fascial system. *J. Bodyw. Mov. Ther*. **20**, 139–140 (2016).

16. Dunkin, C. S. et al. Scarring occurs at a critical depth of skin injury: precise measurement in a graduated dermal scratch in human volunteers. *Plast. Reconstr. Surg*. **119**, 1722–1734 (2007).

17. Koehler, R. H. et al. Minimal adhesions to ePTFE mesh after laparoscopic ventral incisional hernia repair: reoperative findings in 65 cases. *JSLS* **7**, 335–340 (2003).

18. Rippa, A. L., Kalabusheva, E. P., & Vorotelyak, E., A. Regeneration of dermis: scarring and cells involved. *Cells* **8**, 607 (2019).

19. Zamir, E. A., Rongish, B. J. & Little, C. D. The ECM moves during primitive streak formation—computation of ECM versus cellular motion. *PLoS Biol*. **6**, e247 (2008).

20. Szabó, A., Rupp, P. A., Rongish, B. J., Little, C. D. & Czirók, A. Extracellular matrix fluctuations during early embryogenesis. *Phys. Biol*. **8**, 045006 (2011).

21. Aleksandrova, A. et al. Convective tissue movements play a major role in avian endocardial morphogenesis. *Dev. Biol*. **363**, 348–361 (2012).

22. Loganathan, R. et al. Extracellular matrix motion and early morphogenesis. *Development* **143**, 2056–2065 (2016).

23. Miron-Mendoza, M., Koppaka, V., Zhou, C. & Petroll, W. M. Techniques for assessing 3-D cell-matrix mechanical interactions in vitro and in vivo. *Exp. Cell Res*. **319**, 2470–2480 (2013).

24. Sakar, M. S. et al. Cellular forces and matrix assembly coordinate fibrous tissue repair. *Nat. Commun*. **7**, 11036 (2016).

25. Abu-Hijleh, M. F., Roshier, A. L., Al-Shboul, Q., Dharap, A. S. & Harris, P. F. The membranous layer of superficial fascia: evidence for its widespread distribution in the body. *Surg. Radiol. Anat*. **28**, 606–619 (2006).

26. Avelar, J. Regional distribution and behavior of the subcutaneous tissue concerning selection and indication for liposuction. *Aesthetic Plast. Surg*. **13**, 155–165 (1989).

27. Lockwood, T. E. Superficial fascial system (SFS) of the trunk and extremities: a new concept. *Plast. Reconstr. Surg*. **87**, 1009–1018 (1991).